Version R1

Research Communication article

Long-term administration of the mitochondria-targeted antioxidant mitoquinone mesylate fails to attenuate age-related oxidative damage or rescue the loss of muscle mass and function associated with aging of skeletal muscle

Giorgos K Sakellariou[1,2], Timothy Pearson[1], Adam P Lightfoot[1], Gareth A Nye[1], Nicola Wells[1], Ifigeneia I. Giakoumaki[1], Richard D Griffiths[1], Anne McArdle[1] and Malcolm J Jackson[1]*.

Affiliations

[1]MRC-Arthritis Research UK Centre for Integrated Research into Musculoskeletal Ageing, Department of Musculoskeletal Biology, Institute of Ageing and Chronic Disease, University of Liverpool, Liverpool, L693GA, U.K.

[2]Current address: GeneFirst Ltd, Culham Science Centre, Abingdon, Oxfordshire, OX14 3DB, UK.

Running title: Mitoquinone mesylate fails to prevent sarcopenia and age-related oxidative damage

***Corresponding author:**
Prof. M. J. Jackson,
Institute of Ageing and Chronic Disease
University of Liverpool,
Liverpool, L693GA, U.K.
Tel: (44)1517064072,
Fax: (44)151706580,
E-mail: mjj@liverpool.ac.uk

List of Abbreviations

3-NT, 3-Nitrotyrosine; 4-HNE, 4-hydroxynonenal; 8-OHdG, 8-hydroxydeoxyguanosine; AT, anterior tibialis; EDL, extensor digitorum longus; GTN, gastrocnemius; SOL, soleus muscle; B2M, beta-2 microglobulin; BW, body weight CAT, catalase; COX I, cytochrome c oxidase subunit I; COX IV, cytochrome c oxidase subunit IV; CS, citrate synthase; CSA, cross-sectional area; DRP1, dynamin related protein-1; FIS1, mitochondrial fission-1 protein; GAPDH, glyceraldehyde 3-phosphate dehydrogenase; gDNA, genomic DNA; GPX1, glutathione peroxidase 1; H_2O_2, hydrogen peroxide; HSP, heat shock protein; MCIP1, modulatory calcineurin interacting protein-1; MFN1, mitofusin-1; MFN2, mitofusin-2; Mitoquinone mesylate (MitoQ), [10-(4,5-dimethoxy-2-methyl-3,6-dioxo-1,4-cyclohexadien-1-yl)decyl] triphenylphosphonium; mtDNA, mitochondrial DNA; mtROS, mitochondrial ROS; ND1, mitochondrial encoded NADH dehydrogenase-1; nuclear factor kappa B, NFκB; NOS, nitric oxide synthase isoenzymes; NOX4, nicotinamide adenine dinucleotide phosphate oxidase 4; NRF1, nuclear respiratory factor-1; OGG1, oxoguanine DNA glycosylase; OPA1, optic atrophy type-1; PBS, Phosphate Buffered Saline; PECAM 1, platelet endothelial cell adhesion molecule-1; PGC1α, peroxisome proliferator-activated receptor α; PINK1, PTEN-induced putative kinase 1; Poly-UB, polyubiquitin; PRXV, peroxiredoxin V; RCI, respiratory control index; RONS, reactive oxygen and nitrogen species; RPS29, ribosomal protein S29; SOD, superoxide dismutase; TFAM, mitochondrial transcription factor A; TMRM, tetramethylrhodamine, methyl ester fluorescence; TRX, thioredoxin; TRXR, thioredoxin reductase; TPP^+, triphenylphosphonium; UCP, uncoupling protein.

Abstract

Age-related skeletal muscle dysfunction is the underlying cause of morbidity that affects up to half the population aged 80 or over. Considerable evidence indicates that oxidative damage and mitochondrial dysfunction contribute to the sarcopenic phenotype that occurs with aging. To examine this, we administered the mitochondria-targeted antioxidant mitoquinone mesylate (also known as MitoQ, 100μM) to wild-type C57BL/6 mice for 15 weeks (from 24 to 28 mo of age) and investigated the effects on age-related loss of muscle mass and function, changes in redox homeostasis and mitochondrial organelle integrity and function. Here we show that mitoquinone mesylate treatment failed to prevent age-dependent loss of skeletal muscle mass associated with myofiber atrophy or alter a variety of *in situ* and *ex vivo* muscle function analyses including maximum isometric tetanic force, decline in force following a tetanic fatiguing protocol and single fiber specific force. Furthermore, we provide evidence that long-term mitoquinone mesylate administration did not reduce mitochondrial reactive oxygen species nor induce significant changes in muscle redox homeostasis, assessed by changes in 4-hydroxynonenal protein adducts, protein carbonyl content, protein nitration and DNA damage determined by the content of 8-hydroxydeoxyguanosine. Mitochondrial membrane potential, abundance and respiration assessed in permeabilized myofibers was not significantly altered in response to mitoquinone mesylate treatment. Collectively, these findings demonstrate that long-term mitochondria-targeted mitoquinone mesylate administration failed to attenuate age-related oxidative damage in skeletal muscle of old mice or provide any protective effect in the context of muscle aging.

Key words: superoxide, SOD, heat shock proteins, NOX4, NFκB.

Introduction

Age-related loss of muscle mass and function underlies morbidity and mortality that affects up to half the population aged 80 or older (1). Loss of muscle strength in the elderly is a contributor to loss of independence, and physical disability, which is linked with increased risk of falls and fractures. Many structural and functional changes occur with advancing age in skeletal muscle including a reduction in the number and cross-sectional area (CSA) of individual muscle fibers (2).

Oxidative stress has been suggested to be among the factors contributing to the initiation and progression of sarcopenia that occurs during aging (3, 4). Reports from our group (5-11) and others (12, 13) have shown that genetic manipulations of redox regulatory systems modifies the muscle aging process. Skeletal muscle has a high content of mitochondria (14) and mitochondrial redox homeostasis has been proposed to play a key role in age-related oxidative damage (15). Consistent with a role of mitochondria as a contributor to age-related muscle redox changes, studies have shown that isolated skeletal muscle mitochondria exhibit an age-dependent increase in hydrogen peroxide (H_2O_2) generation (16, 17).

Reactive oxygen species (ROS) derived from mitochondria (mtROS) are linked to the pathogenesis of a number of age-related human diseases including neurodegenerative disorders, ischemia-reperfusion injury and diabetes (18, 19). Considerable evidence has shown that mitochondrial oxidative damage can alter mitochondrial integrity and function in aging skeletal muscle including a reduction in mitochondrial abundance (20) and oxidative-phosphorylation (21), accumulation of mutated mtDNA (15) associated with impaired mitophagy (22), and increased mitochondrial-mediated apoptosis (23) which could all contribute to sarcopenia. Although cumulative oxidative damage has been suggested to induce age-associated decline in mitochondrial function (24), the effects of mitochondrial dysfunction and mtROS in age-related muscle atrophy remains a controversial topic (25, 26).

To directly examine whether age-related atrophy and mitochondrial dysfunction is related to mitochondrial redox changes, we administered the mitochondria-targeted antioxidant mitoquinone mesylate (also known as MitoQ): [10-(4,5-dimethoxy-2-methyl-3,6-dioxo-1,4-cyclohexadien-1-yl)decyl] triphenylphosphonium to 24 mo old mice for 15 weeks and investigated the effects on age-related loss of muscle mass and function, changes in muscle redox homeostasis, mitochondrial organelle function and content. We hypothesized that if alterations in the mitochondrial redox status are implicated in the processes of age-related muscle wasting, mitoquinone mesylate drug treatment would ameliorate the sarcopenic phenotype associated with loss of muscle mass and

weakness. In the present study we report the effects of long-term administration of mitoquinone mesylate on muscle mass, morphology and function, redox homeostasis, adaptive responses and mitochondrial integrity and function in aging skeletal muscle.

Materials and Methods

Chemicals and Reagents. Unless stated otherwise, all chemicals used in this study were obtained from the Sigma Chemical Company.

Mice. Male and female WT C57Bl/6 mice (8 mo old) were obtained from Charles River Laboratories (Margate, UK) and aged to 28 mo at the Biomedical Services Unit, University of Liverpool. All experiments were conducted in accordance with UK Home Office guidelines under the UK Animals (Scientific Procedures) Act 1986. Mice were fed a CRM (P) rodent diet and were maintained under barrier conditions in microisolator cages on a 12-h dark/light cycle. For simple tissue collection, mice were euthanized by cervical dislocation, and muscles/tissues were either rapidly removed, snap-frozen, and stored at -80°C, or embedded in Tissue-Tek (VWR) and rapidly frozen in nitrogen-chilled isopentane for histological analysis. Mice subjected to *in situ* muscle force measurements were anesthetized with intraperitoneal (IP) injections of ketamine hydrochloride (66 mg/kg) and medatomidine hydrochloride (0.55 mg/kg), with supplemental injections provided to maintain an adequate level of anaesthesia throughout the procedure. All procedures were approved by the University of Liverpool Animal Welfare and Ethical Review Body.

Mitoquinone mesylate administration. Mice were 24 mo of age at the start of the treatment and were administered 100μM mitoquinone mesylate (as a β-cyclodextrin complex, supplied by Suzhou Vosun Chemical, China) in their drinking water for the subsequent 15 weeks. Fresh mitoquinone mesylate solutions were given twice a week, control mice were supplied with water without the supplement (n=8 mice/group). All mice were monitored daily and weighed once a week. We selectively chose to administer mice with mitoquinone mesylate between the age of 24 to 28 mo old since preliminary studies (Fig. 1A) showed that age-related muscle atrophy became apparent over the time period of 24-28 mo. The dosage of mitoquinone mesylate used in the present study was based on that previously used (100μM) to protect against oxidative damage in a mouse model of Alzheimer's disease (27). Other previous studies have used mitoquinone mesylate doses as high as 500μM for up to 28 weeks (28).

***In situ* muscle function analysis.** Extensor digitorum longus (EDL) muscle contractile properties were measured *in situ* as previously described (5). To assess the maximum isometric tetanic force (P_o) of the EDL muscle, the distal tendon from anesthetized mice was severed and secured to the lever arm of a servomotor (Aurora Scientific). The knee of the hindlimb was fixed, the peroneal nerve was exposed, and bipolar platinum wire electrodes were placed across the nerve. Muscle optimal length (L_o) was determined using a series of 1 Hz stimulation and set at the length that generates the maximal force. For determination of P_o, EDL muscles were electrically stimulated to contract at L_o and optimal stimulation voltage (8–10 V) at 2min intervals for 300ms with 0.2ms pulse width. P_o was assessed by increasing the frequency of stimulation from 10 to 50 Hz and, subsequently, in 50-Hz increments to a maximum of 300Hz. P_o was identified when the maximum force reached a plateau, despite increasing stimulation frequency. After identification of P_o, mice were subjected to a repetitive tetanic fatiguing protocol, which consisted of 60 consecutive isometric contractions (300ms at 100Hz every 5sec for 5min) (29). Following completion of the procedures, mice were killed by cervical dislocation, and muscles/tissues were rapidly removed. Muscle fiber length (L_f) and weight of EDL muscles were measured *ex vivo* to determine muscle cross-sectional area (CSA). Specific P_o (mN/mm^2) was calculated by dividing P_o by total fiber CSA for each muscle.

Determination of muscle structure. Anterior tibialis (AT) muscles were cryosectioned at -20°C through the mid-belly with a thickness of 12µm, and fluorescent immunohistochemical (IHC) staining was undertaken on the same day. Sections were rinsed with Phosphate Buffered Saline (PBS) and permeabilized in 0.2% Triton X-100 in PBS for 5min. Fluorescein labelled wheat germ agglutinin (Vector Laboratories, 5µg/ml) was used to identify extracellular matrix. Nuclei were identified using 4',6-diamidino-2-phenylindole (DAPI, 1µg/ml). Cross sections from 5-6 muscles/treatment group were examined by blinded observers to count the total number of fibers, percentage of centronucleated fibers and individual fiber CSA. To ensure that all fibers/section were analysed, consecutive images acquired from each cryosection at 10x magnification were merged into a single high-resolution image using Adobe photoshop CS5 (see Fig. 1B). Image J software was used to quantify individual fiber CSA.

Confocal laser scanning microscopy. Fluorescence images were obtained using a C1 confocal laser scanning microscope (Nikon) equipped with a 405nm excitation diode laser, a 488nm excitation argon laser, and a 543nm excitation helium-neon laser. Emission fluorescence was detected through a set of 450/35, 515/30, and 605/15 emission filters. Fluorescence images were analyzed with the EZC1 V.3.9 (12bit) acquisition software.

Preparation of permeabilized muscle fiber bundles. Selective plasma membrane permeabilization of fiber bundles was performed according to methods described by Kuznetsov *et al* (30) to allow analysis of intact skeletal muscle mitochondria *in situ* (19, 31). In brief, AT muscles were placed in ice-cold buffer A, containing (in mM) 50 K-MES, 7.23 K_2EGTA, 2.77 CaK_2EGTA, 20 imidazole, 0.5 DTT, 20 taurine, 5.3 Na_2ATP, 15 PCr, and 6.56 $MgCl_2$-$6H_2O$ (pH 7.3 at 4°C) and trimmed of connective tissue and fat. Muscles were manually teased into small bundles of fibers and treated with 50µg/ml saponin (in buffer A) for 30min at low rocking speed. Following permeabilization, fiber bundles prepared for mitochondrial H_2O_2 emission measurements, were washed 3x10min in ice-cold buffer Z, containing (in mM) 110 K-MES, 35 KCl, 1 EGTA, 5.3 Na_2ATP, 10 K_2HPO_4, and 3 $MgCl_2$-$6H_2O$ (pH 7.3 at 4°C), supplemented with 5mg/ml BSA. Permeabilized fiber bundles prepared for respiration analyses were washed 3x10min in ice-cold buffer B containing, (in mM) 100 K-MES, 7.23 K_2EGTA, 2.77 CaK_2EGTA, 20 imidazole, 0.5 DTT, 20 taurine, 3 K_2HPO_4, and 1.38 $MgCl_2$-$6H_2O$ (pH 7.3 at 4°C), supplemented with 2mg/ml BSA.

***Ex vivo* single muscle fiber analysis.** Isolated intact single muscle fibers were excised from the AT muscle and maintained in ice-cold relax solution, containing (in mM) 4.5 MgATP, 1 free Mg^{2+}, 10 imidazole, 2 EGTA, and 100 KCL (pH 7.0) (32). Single fibers were permeabilized with 50µg/ml saponin (in relax solution) for 15min on ice. Permeabilized fibers were mounted on an 802D muscle testing apparatus (Aurora Scientific), mounted upon insect pins with fine thread, attached to a 403A (5mN) force transducer and 312C length controller (see Fig. 8H). Single fibers were maximally activated (pCa 4.5) ([-log[free Ca2+]) containing: (in mM) 5.3 MgATP, 1 free Mg^{2+}, 20 imidazole, 7 EGTA, 19.6 PCr, and 64 KCl (pH 7.0). Maximal force was recorded for each fiber and normalized to CSA (32). Sarcomere length for each individual myofiber was adjusted to 2.4-2.6µm and diameter measured at four intervals along the length of the fiber, and circular circumference assumed for the calculation of CSA.

Mitochondrial respiration analysis. Permeabilized myofiber respiration was assessed using a Clark-type electrode in a continuously stirred sealed and thermostatically controlled chamber (Oxytherm System, Hansatech Instruments Ltd.) maintained at 37°C. Following calibration of the respiration chamber, permeabilized bundles (~15mg wet weight) were incubated in respiration buffer B (22, 31). Respiration (O_2 consumption) was determined using glutamate (5mM) and malate (5mM) substrates (G/M). ADP-stimulated respiration (state 3) was initiated by addition of ADP (0.3mM). Respiratory control index (RCI) was calculated by dividing state 3 by state 4 respiration and the efficiency of oxidative phosphorylation was determined by calculating the ratio of ATP amount to consumed O_2 during state 3 respiration (P:O ratio).

Mitochondrial H_2O_2 emission measurements. Mitochondrial H_2O_2 efflux was measured using the Amplex Red-horseradish peroxidase (HRP, Molecular Probes) assay as previously described (16). H_2O_2 production was expressed as picomoles per minute per unit of Citrate Synthase (CS) activity.

Mitochondrial DNA quantification. Mitochondrial DNA (mtDNA) was measured by quantitative RT-PCR (qRT-PCR) as described by Chen *et al* (33).

DNA damage and DNA fragmentation. DNA damage was assessed by the content of 8-hydroxydeoxyguanosine (8-OHdG) as described recently by Changou *et al* (34). Apoptotic DNA fragmentation was assessed by DNA laddering using agarose gel electrophoresis as described by Houot *et al* (35).

Fluorescence-based methods to measure mitochondrial membrane potential and MitoSOX Red oxidation. To monitor changes in mitochondrial superoxide, isolated fibers from the AT muscle were loaded with MitoSOX Red (250nM, Invitrogen) for 30min as previously described (36). Fibers were maintained in buffer Z containing MitoSOX Red (20nM) during the experimental period. The reaction between superoxide and MitoSOX Red generates a specific red fluorescent product, 2-hydroxyethidium (2-OH-Mito-E^+) (37), monitored at an excitation/emission wavelength of 405/605nm (see Fig. 2A). Measurement of mitochondrial membrane potential ($\Delta\Psi m$) in intact mitochondria of isolated AT fibers was assessed by tetramethylrhodamine, methyl ester (TMRM, 30nM, Invitrogen) fluorescence at an excitation/emission wavelength of 543/605nm (see Fig. 6C). Changes in $\Delta\Psi m$ were determined in the presence of oxidative phosphorylation inhibitors; oligomycin (Olm, 2.5μM) and FCCP (4μM) as indicated in schematic Fig. 6C.

Enzymatic activity assays. Enzymatic activity of CuZnSOD and MnSOD was assessed in native gels, with negative staining (see Fig. 2H), as described previously (6, 8). Aconitase activity was quantified by measuring the reduction of $NADP^+$ to NADPH following addition of 2U of isocitrate dehydrogenase by using a microplate fluorometer (FLUOstar Optima, BMG) at an excitation/emission wavelength of 360/460nm (38). Mitochondrial enzyme citrate synthase (CS) activity was determined spectrophotometrically using the MitoCheck Citrate Synthase Activity Assay (Cayman Chemicals) according to manufacturer's protocol. Respiratory chain complex I activity in skeletal muscle homogenates was examined by the reduction of 2,6-dichloroindophenol (DCIP), followed spectrophotometrically at 600nm as described by Janssen *et al* (39).

Quantitative RT-PCR analysis. RNA from skeletal muscle was extracted, DNase-treated and purified using Direct-zol RNA miniprep (Zymo Research). Purified RNA was utilised to generate first-strand cDNA using the

iScript cDNA Synthesis kit (Bio-Rad). Primers for qRT-PCR analyses are shown in Table 1 and the optimal annealing temperature for each primer set was determined by using an annealing temperature gradient between 55 and 62°C. Real-time PCR reactions were performed on an iCycler Detection System (Bio-Rad) using iQ SYBR Green Supermix (Bio-Rad). Specificity of the PCR products was determined by melt curve analysis and agarose gel electrophoresis. Three reference genes including GAPDH, beta-2-microglobulin (B2M) and ribosomal protein S29 (RPS29) were used as internal controls.

Immunoblotting. Protein extracts (20μg/sample) were separated using a standard protocol for western blots (7). Peroxidase activity was detected using an ECL kit (Amersham International), and band intensities were analysed using Quantity One Software (Bio-Rad). Mitochondrial and cytosolic sub-cellular fractions were obtained from skeletal muscle as previously described (40).

Statistical Analyses. Data are presented as mean ± SEM for each experiment. Statistical analyses for potential differences between groups were determined using analysis of variance (ANOVA) followed by the *post hoc* LSD test. Single comparisons between two experimental conditions were undertaken using the unpaired Student's t test. Data were analysed using SPSS 22 and p values of less than 0.05 were considered statistically significant.

Results

Age-related loss of muscle mass is associated with myofiber atrophy. To determine the time-course of age-related phenotypic changes that occur in skeletal muscle, we initially assessed anterior tibialis (AT) muscle mass at 12, 18, 24 and 28 months of age in mice (Fig. 1A). AT muscle showed age-related loss of muscle mass (~34% reduction in mass relative to body weight) at 28 mo of age (Fig. 1A). To understand the structural muscle changes underlying sarcopenia, immunohistochemical analysis of AT muscle (Fig. 1B) was undertaken for 18 and 28 mo old mice. The total number of fibers/AT muscle tended to be reduced by a mean of ~11% in 28 mo old mice in comparison with 18 mo old mice (Fig. 1C) but the changes were not significantly different. We then examined whether AT muscle of 28 mo old mice showed atrophy of the remaining muscle fibers (Fig. 1D). Average muscle fiber cross-sectional area (CSA) was reduced significantly by a mean ~46% from 18 to 28 mo of age suggesting that myofiber atrophy is the predominant cause of the loss of skeletal muscle mass that occurs between these ages.

Long-term administration of mitochondria-targeted antioxidant mitoquinone mesylate fails to attenuate age-related mtROS increase in muscle fibers from old mice. Previous studies from our group (16) and others (17) have shown that isolated skeletal muscle mitochondria exhibit an age-related increase in hydrogen peroxide (H_2O_2), which is associated with increased mitochondrial oxidative damage (21). To assess whether age-dependent mtROS increase and oxidative damage are contributing factors to the loss of muscle mass that occurs with aging, 24 mo old mice were treated with mitochondria-targeted mitoquinone mesylate for 15 weeks. We chose to administer the compound between the ages of 24 to 28 mo old since our data (Fig. 1A) revealed that loss of muscle mass occurs post 24 mo of age. To assess the antioxidant effect of mitoquinone mesylate, single muscle fibers isolated from the AT muscle of control and mitoquinone mesylate-treated old mice were loaded with MitoSOX Red (Fig. 2A, top). Mitoquinone mesylate treatment was found to increase the 2-OH-Mito-E^+ fluorescence (Fig. 2A, bottom) indicating a potential increase in mitochondrial superoxide productio. To further assess changes in mtROS, in the presence of mitochondrial substrates and inhibitors, we determined H_2O_2 efflux from intact mitochondria in permeabilized myofibers from the AT muscle (Fig. 2B, C). Saponin-permeabilized fibers from the AT muscle displayed good morphology and well-defined striations along the sarcolemma and stained positive for TO-PRO-1 iodide indicating plasma membrane permeabilization (Fig. 2B). Glutamate/malate (complex I substrates) and succinate (complex II substrate) fuelled mitochondria from treated old mice showed a tendency towards a higher increase in H_2O_2 emission compared with control old mice (Fig. 2C), but did not reach statistical significance. The succinate induced H_2O_2 release was abolished by the complex I inhibitor, rotenone, suggesting that this H_2O_2 release likely derives from complex I (Fig. 2C).

As these results were unexpected, we next sought to determine whether long-term administration of mitoquinone mesylate altered the expression of potential sources for mtROS generation including complex I, II, III (41) and mitochondrial nicotinamide adenine dinucleotide phosphate oxidase 4 (NOX4), (14, 36). To assess mitochondrial protein levels of NOX4, mitochondrial and cytosolic fractions from skeletal muscle of control and mitoquinone mesylate-treated old mice were prepared (Fig. 2E). We observed no changes in protein expression of complex I, II and III (Fig. 2D) or mtNOX4 (Fig. 2F). Similarly, no changes were observed in the enzymatic activities of respiratory complex I (Fig. 2G) or mitochondrial matrix superoxide dismutase 2 (SOD2) (Fig. 2H). A tendency to a reduction in SOD1 activity was observed in skeletal muscle of mitoquinone mesylate-treated old mice compared to control old mice, ($p=0.06$). These findings were somewhat surprising, but indicate that long-term mitoquinone mesylate treatment of old mice failed to attenuate the age-related increase in ROS generation by intact mitochondria in isolated skeletal muscle fibers.

Mitoquinone mesylate fails to attenuate oxidative damage in aging skeletal muscle. To determine if long-term mitoquinone mesylate treatment altered levels of age-related oxidative damage in skeletal muscle (42-44), we next examined the amounts of protein oxidation, lipid peroxidation, DNA damage and protein nitration (Fig. 3A-D). Mitoquinone mesylate treatment tended to increase age-related protein carbonylation (9) in whole AT muscle (Fig. 3A, top left), and mitochondrial fractions (Fig. 3A, top right). There was also a tendency for an increase in protein carbonyl content of cytosolic fractions from mitoquinone mesylate-treated mice (Fig. 3A, bottom). Assessment of lipid peroxidation in mitochondrial and cytosolic fractions from skeletal muscle of control and mitoquinone mesylate-treated old mice was undertaken by immunoblotting for 4-hydroxynonenal (4-HNE) protein adducts (Fig. 3B). The data obtained were similar to those for protein oxidation in that mitoquinone mesylate-treatment tended to increase lipid peroxidation in both fractions (Fig. 3B). However, neither protein carbonylation nor lipid peroxidation markers showed statistically significant differences between control and mitoquinone mesylate-treated mice. The extent of oxidative DNA damage was also assessed by examining 8-hydroxydeoxyguanosine (8-OHdG) in genomic DNA and protein expression of oxoguanine DNA glycosylase (OGG1), a primary enzyme responsible for the excision of 7, 8-dihydro-8-oxoguanine lesion (45), (Fig. 3C). Muscle from mitoquinone mesylate-treated old mice showed a trend towards a reduction ($p=0.09$) in OGG1 protein levels (Fig. 3C, right/bottom), with no change in the levels of 8-OHdG (Fig. 3C, left). Finally, the level of protein nitration (3-NT) and the expression of peroxiredoxin V (PRXV), a peroxynitrite reductase (7), were determined (Fig. 3D), but no effects on 3-NT content (Fig. 3D, left) or PRXV expression (Fig. 3D, right/bottom) were observed. Overall, these data indicate that long-term administration of mitoquinone mesylate did not reduce oxidative damage in muscle of old mice.

Mitoquinone mesylate alters the expression of redox regulatory proteins in aging skeletal muscle. To determine whether long-term mitoquinone mesylate treatment of old mice caused adaptations in the expression of proteins involved in antioxidant defence, we measured the expression of redox regulatory proteins including; superoxide dismutase (SOD) isoforms (Fig. 4A), nitric oxide synthase (NOS) isoenzymes (Fig. 4B), H_2O_2 scavenging enzymes including glutathione peroxidase 1 (GPX1), catalase (CAT) and PRXIII (Fig. 4C), redox proteins involved in the thioredoxin-peroxiredoxin (TRX-PRX) system (Fig. 4D) and heat shock proteins (HSPs), (Fig. 4E) which have all been shown to provide protection against the damaging effects of increased RONS production (6, 9). Densitometric quantification (Fig. 4F) of the blots presented in Fig. 4A-E revealed a significant reduction in protein expression of extracellular SOD3 isoform and mitochondrial SOD1. This was also associated with a trend towards increased levels of TRX-PRX regulatory proteins including thioredoxin reductase 1 (TRXR1), mitochondrial TRXR2, iNOS (the inducible isoform of NOS) and a reduction in HSC70 (Fig. 4F). The NFκB signalling pathway is known to regulate the expression of iNOS (46) and ROS antioxidant

enzymes (4) and previous *in vitro* studies have demonstrated enhanced NFκB activation following incubation with mitoquinone mesylate (47), we therefore examined activation of the NFκB pathway which we have previously shown to be increased in skeletal muscle of old mice (48). Muscle of mitoquinone mesylate-treated old mice showed no significant change in activation of the NFκB pathway as indicated by phosphorylation of IκB-α (Phospho IκB-α), total IκB-α content (a key inhibitor of NFκB activation) or NFκB-P65 protein content (total and phosphorylated), (Fig. 4G). Overall, these data suggest that long-term treatment of mitoquinone mesylate may have altered the expression of a small number of specific redox regulatory proteins in skeletal muscle from old mice.

Long-term mitoquinone mesylate treatment does not affect mitochondrial abundance in skeletal muscle of old mice. We sought to determine whether mitoquinone mesylate-treated old mice showed a change in mitochondrial abundance (15, 20), (Fig. 5A, B). Muscle of treated old mice showed a tendency to a reduction in mitochondrial DNA (mtDNA) copy numbers per nuclear genome (Fig. 5A) and citrate synthase activity (Fig. 5B). Quantitative RT-PCR analysis of expression of genes involved in mitochondrial dynamics (fusion and fission) and biogenesis (Fig. 5C, top) showed that mRNA levels were similar between muscle of mitoquinone mesylate-treated and control old mice (Fig. 5C, bottom). Protein levels of the transcriptional coactivator and regulator of mitochondrial biogenesis, peroxisome proliferator-activated receptor α (PGC-1α) did not differ between control and mitoquinone mesylate-treated old mice (Fig. 5D). A potential effect on mitophagy was investigated using isolated mitochondrial fractions from skeletal muscle of control and mitoquinone mesylate-treated old mice immunoblotted for PTEN-induced putative kinase 1 (PINK1), and ubiquitin ligase Parkin mitophagy markers (Fig. 5E). We observed increased recruitment of PINK1, but no significant difference in Parkin in isolated mitochondria from mitoquinone mesylate-treated old mice (Fig. 5E) compared with values from control old mice, suggesting an increased mitophagic response. Levels of Sirtuin 1 (Sirt1), (Fig. 5D), an important regulator of mitochondrial recycling through the process of autophagy (49) were unchanged in the treated mice.

Long-term mitoquinone mesylate treatment does not influence the mitochondrial membrane potential in intact mitochondria of permeabilized muscle fibers in old mice. Cumulative oxidative damage has been proposed to induce age-associated reductions in mitochondrial function (24, 50), thus we investigated mitochondrial function in skeletal muscle of mitoquinone mesylate-treated old mice (Fig. 6A-E). Skeletal muscle of mitoquinone mesylate-treated old mice exhibited similar levels of mitochondrial aconitase activity (Fig. 6A) and mitochondrial protein levels (Fig. 6B, top right) compared with control old mice, although a tendency to a reduction in aconitase content ($p=0.06$) was observed in the cytosolic compartment of the AT

muscle (Fig. 6B, bottom left). The mitochondrial membrane potential ($\Delta\Psi m$) of intact mitochondria in isolated AT muscle fibers was examined by changes in tetramethylrhodamine, methyl ester (TMRM) fluorescence (Fig. 6C, top) following treatment with oligomycin and the protonophore, FCCP (Fig. 6C, middle). Statistical analysis of the area under the TMRM fluorescence trace did reveal differences between mitoquinone mesylate-treated and control old mice (Fig. 6C, bottom). Next, we evaluated mitochondrial respiratory function in saponin-permeabilized fiber bundles following addition of glutamate/malate substrates and ADP. Myofibers from mitoquinone mesylate administered old mice showed a trend towards a reduction ($p=0.17$) in respiratory control index (RCI), (Fig. 6D, left) associated with a trend towards increased uncoupling protein 2 (UCP2) protein levels ($p=0.06$), (Fig. 6E). No changes in P:O ratio (Fig. 6D, right) or UCP3 protein expression (Fig. 6E) were observed in mitoquinone mesylate-treated old mice compared with control old mice.

Mitochondrial-mediated apoptosis is not altered in response to long-term mitoquinone mesylate treatment in aging skeletal muscle. A variety of pro-apoptotic markers were examined including expression of BAK, BAX and VDAC1 (Fig. 7A), proteolytic enzymes linked to apoptosis including expression of calpain I and calpastatin (Fig. 7B), mitochondrial release of cytochrome c and Smac/DIABLO pro-apoptotic proteins to cytosol (Fig. 7C), mitochondrial endonuclease G (Fig. 7D) and DNA fragmentation of genomic DNA (gDNA), (Fig. 7E). These results showed no changes in mitochondrial-mediated apoptotic processes in response to mitoquinone mesylate treatment.

Long-term administration of mitoquinone mesylate failed to prevent the loss of muscle mass and function that occurred with aging. We first examined whether long-term mitoquinone mesylate treatment affected muscle mass and structure in old mice. The trend lines depicted in Fig. 8A showed no changes in body weight (BW) during the 15-week treatment. The tissue weights of several skeletal muscles and organs did not differ significantly between control and mitoquinone mesylate-treated old mice (Table 2), although there was a trend towards reduced spleen mass ($p=0.12$) and increased kidney mass ($p=0.1$). To assess changes in muscle morphology, transverse sections of AT muscle from control and mitoquinone mesylate-treated old mice were double immunolabeled with WGA, to visualize extracellular matrix, and DAPI, to mark nuclei (Fig. 8B). Histological analysis revealed no changes in number of centrally-nucleated fibers (Fig. 8C, left), total number of fibers/AT muscle (Fig. 8C, right) or average muscle CSA (Fig. 8C, bottom) in response to the mitoquinone mesylate treatment. Quantitative analysis of individual fiber CSA showed no differences in myofiber size (Fig. 8D) or fiber type distribution (Fig. 8E) of AT or gastrocnemius (GTN) skeletal muscles between control and mitoquinone mesylate-treated old mice. Next, we examined the effect of mitoquinone mesylate administration on age-related changes in muscle function (5, 17), (Fig. 8F-J). Functional measurements of extensor digitorum

longus (EDL) muscle force production *in situ* revealed no changes in maximum isometric specific force between control and mitoquinone mesylate-treated old mice (Fig. 8F). *In situ* measurements of the decline in force generation by EDL muscles during a series of repeated isometric contractions revealed a trend towards a greater decline in force in mitoquinone mesylate-treated mice compared with values from control old mice (Fig. 8G), but the apparent greater decline in the mitoquinone mesylate treated mice (Fig. 8G) was not statistically different. Finally, to evaluate the force production at the single-fiber level, we recorded *ex-vivo* muscle force of single isolated skinned fibers (Fig. 8H) obtained from the AT muscle. This allowed us to examine the force generated by sarcomeric proteins independent of innervation, fiber number, ATP levels and calcium release (51). Neither specific force (Fig. 8I) nor the time to peak maximum tension (Fig. 8J) differed between the control and mitoquinone mesylate-treated old mice. Collectively, these data reveal that long-term mitoquinone mesylate treatment did not alter age-related muscle atrophy, or any of functional deficits associated with aging skeletal muscle.

Discussion

Considerable evidence has indicated that skeletal muscle decline with advancing age is associated with an increased oxidative status in redox-responsive proteins (52) and increased oxidative modifications of macromolecules including DNA, proteins and lipids (4). Altered mitochondrial redox homeostasis has been proposed to play-a key role in sarcopenia (19, 21, 53) and skeletal muscle mitochondria have been reported to exhibit an age-dependent increase in mtROS (16, 17). Aging of skeletal muscle is associated with mitochondrial dysfunction including reduced maximal ATP-generating capacity, impaired function of the mitochondrial permeability transition pore and reduced maximal respiratory capacity (21, 31). Although cumulative oxidative damage has been suggested to induce age-associated decline in mitochondrial function (24), the effect of mitochondrial dysfunction and mtROS as the underlying key regulators of the age-related atrophy process remains an area of active research (25, 26).

Skeletal muscle produces ROS from a variety of subcellular sites (14) and studies assessing the potential role of mtROS as the underlying mechanism of mitochondrial dysfunction and muscle wasting have been restricted, in part, by a the lack of interventions to selectively target mtROS. In the current study we determined the time-course of age-related phenotypic/structural changes that occur in skeletal muscle and assessed the contribution of mtROS by utilizing the mitochondria-targeted ubiquinone derivative mitoquinone mesylate, which may selectively protect mitochondria from oxidative damage.

Data indicate that age-related loss of muscle mass occurred post 24 mo of age in these C57Bl mice, and was attributed to a significant reduction in fiber CSA, when compared with 18 mo old mice. Our findings are in agreement with recent human studies, highlighting age-dependent fiber atrophy as a primary cause of loss of muscle mass with advancing age (22).

Previous work from our group (16) and others (17) has shown that age-dependent loss of muscle mass and function is associated with increased mitochondrial H_2O_2 emission and oxidative damage (21), suggesting that changes in mitochondrial redox homeostasis towards an oxidized state may be a contributor to skeletal muscle aging. To directly assess the effect of age-related changes in the mitochondrial redox environment, we used a long-term drug intervention approach, with use of mitoquinone mesylate. This compound has been developed as a therapy for humans and has undergone phase I and II clinical trials (28) and it comprises a ubiquinone moiety covalently attached through an aliphatic ten-carbon chain to triphenylphosphonium (TPP^+), a lipophilic cation that accumulates several-hundred fold within mitochondria (54, 55). Mitoquinone mesylate is absorbed/bound to the matrix-facing surface of the inner mitochondrial membrane (into the hydrophobic core of the phospholipid bilayer) (54), driven by the membrane potential and there it is thought to be continually recycled to the active ubiquinol antioxidant by complex II of the respiratory chain (28).

We assessed the potential of mitoquinone mesylate to rescue myofiber atrophy observed between 24 to 28 mo of age and provide evidence that drug treatment failed to prevent the age-related reduction in fiber CSA. We then examined the effect of long-term administration of mitoquinone mesylate to attenuate age-dependent changes in mtROS and redox homeostasis. To our surprise, mitoquinone mesylate treatment did not reduce mtROS or provide clear antioxidant protective effects, and in contrast we observed an increase in MitoSOX oxidation in the treated mice. Recent *in vitro* studies using skeletal muscle C2C12 cells have also provided similar results, palmitate-induced ROS production was further increased in response to mitoquinone mesylate treatment (56). Thus, the lack of any substantial antioxidant effects in response to mitoquinone mesylate administration did not allow us to directly address the original question posed in the current study: if age-dependent changes in mitochondrial redox homeostasis play a major role in age-related muscle atrophy.

Skeletal muscle of mitoquinone mesylate-treated old mice showed some alterations in the expression levels and activity of RONS regulatory systems and elevated mitophagic potential. We further addressed if mitoquinone mesylate influenced age-related changes in mitochondrial function and muscle force. We found that long-term administration of mitoquinone mesylate did not significantly alter mitochondrial function or muscle function though there was a tendency to adversely affect mitochondrial respiration and the decline in force during a

series of repeated isometric contractions. It is noteworthy that neither of these analyses reached statistical significance. In relation to this, recent *in vitro* studies using state-of-the-art respirometer technology (Seahorse Bioscience) have reported decreased mitochondrial respiration (56) and respiratory uncoupling (57) in skeletal muscle C2C12 myoblasts and endothelial cells in response to mitochondria-targeted coenzyme Q analogs.

The relative increase in mitoSOX oxidation indicating increased mtROS seen in response to long-term administration of mitoquinone mesylate *in vivo* may be related to the quinone group, which has previously been shown to participate in redox cycling (53, 58). Quinone-containing compounds may undergo one-electron reduction by flavin-containing enzymes to form semiquinone radicals, which in turn may rapidly react with O_2 to produce superoxide (59, 60). The work presented in this study indicated that mitochondrial superoxide production, assessed via changes in MitoSOX Red fluorescence, was increased in response to the drug-treatment. Other *in situ* and *in vitro* studies have also provided evidence that mitoquinone mesylate can augment mtROS production by complex I (58, 61) and previous work using sub-mitochondrial particles and purified mitochondrial complex I also suggested that redox cycling of mitoquinone mesylate can occur at the two sites on complex I, proximal and distal to the rotenone-binding site (53).

Potential pro-oxidant effects of mitoquinone mesylate *in vivo* may also potentially be explained by the localisation of its large hydrophilic core in the aqueous phase. Factors that favor superoxide production by ubiquinones are reduction to the ubiquinol and the extent to which they are present in the aqueous environment (28, 62). Deprotonation of ubiquinol, the reduced form of mitoquinone mesylate, in the aqueous phase could lead to an oxidation reaction of quinol, generating superoxide (53, 62). These potential mechanisms offer plausible explanations why the current study has indicated that long-term mitoquinone mesylate treatment enhanced mtROS production in skeletal muscle of old mice.

Previous *in vivo* studies have subjected rodents to long-term administration of mitoquinone mesylate in WT C57BL/6 (28) as well as a transgenic mouse model of Alzheimer's disease (27) and have showed either antioxidant-protective effects (27), or lack of changes in redox homeostasis (28) in brain, liver and cardiac tissue. Both of these studies used young mice, at 4-8 weeks of age and the responses of tissues to this compound may potentially change in old organisms. Alternatively, it is possible that the inherent differences in specific tissue redox potential may alter the efficacy of mitoquinone mesylate in protecting mitochondria from oxidative damage.

To our knowledge this is the first study to utilize a long-term mitoquinone mesylate pharmacological approach and examine the effect on skeletal muscle mitochondrial redox homeostasis, organelle integrity and function as well as age-related loss of muscle mass and function that occurs with aging. We show that mitoquinone mesylate failed to attenuate age-related oxidative damage or rescue the sarcopenic phenotype and functional deficits associated with aging of skeletal muscle.

Acknowledgements

We thank Carol S. Davis and Susan V. Brooks (University of Michigan, USA), Michael E. Walsh (University of Texas Health Science Center, USA), Holly Van Remmen (Oklahoma Medical Research Foundation, USA), Russell T. Hepple (McGill University Health Centre, Canada), Martin Picard (Center for Mitochondrial and Epigenomic Medicine, Philadelphia, USA), Martin Brand (Buck Institute for Research on Aging, Novato, USA), Vladimir P. Skulachev (Moscow State University, Russia), Sergey I. Dikalov (Vanderbilt University Medical Center, USA) and William I. Sivitz (University of Iowa Carver College of Medicine, USA). This work was supported by the Medical Research Council, UK (Grant No: G1002120) and the United States National Institute on Aging (Grant No: AG-20591).

References

1. Umanskaya, A., Santulli, G., Xie, W., Andersson, D. C., Reiken, S. R., and Marks, A. R. (2014) Genetically enhancing mitochondrial antioxidant activity improves muscle function in aging. *Proceedings of the National Academy of Sciences of the United States of America* **111**, 15250-15255
2. Kirkendall, D. T., and Garrett, W. E., Jr. (1998) The effects of aging and training on skeletal muscle. *Am J Sports Med* **26**, 598-602
3. Jackson, M. J. (2013) Interactions between reactive oxygen species generated by contractile activity and aging in skeletal muscle. *Antioxid Redox Signal*
4. Powers, S. K., and Jackson, M. J. (2008) Exercise-induced oxidative stress: cellular mechanisms and impact on muscle force production. *Physiol Rev* **88**, 1243-1276
5. McArdle, A., Dillmann, W. H., Mestril, R., Faulkner, J. A., and Jackson, M. J. (2004) Overexpression of HSP70 in mouse skeletal muscle protects against muscle damage and age-related muscle dysfunction. *FASEB journal : official publication of the Federation of American Societies for Experimental Biology* **18**, 355-357
6. Sakellariou, G. K., Davis, C. S., Shi, Y., Ivannikov, M. V., Zhang, Y., Vasilaki, A., Macleod, G. T., Richardson, A., Van Remmen, H., Jackson, M. J., McArdle, A., and Brooks, S. V. (2014) Neuron-specific expression of CuZnSOD prevents the loss of muscle mass and function that occurs in homozygous CuZnSOD-knockout mice. *FASEB journal : official publication of the Federation of American Societies for Experimental Biology* **28**, 1666-1681
7. Sakellariou, G. K., Pye, D., Vasilaki, A., Zibrik, L., Palomero, J., Kabayo, T., McArdle, F., Van Remmen, H., Richardson, A., Tidball, J. G., McArdle, A., and Jackson, M. J. (2011) Role of superoxide-nitric oxide interactions in the accelerated age-related loss of muscle mass in mice lacking Cu,Zn superoxide dismutase. *Aging cell* **10**, 749-760
8. Zhang, Y., Davis, C., Sakellariou, G. K., Shi, Y., Kayani, A. C., Pulliam, D., Bhattacharya, A., Richardson, A., Jackson, M. J., McArdle, A., Brooks, S. V., and Van Remmen, H. (2013) CuZnSOD gene deletion targeted to skeletal muscle leads to loss of contractile force but does not cause muscle atrophy in adult mice. *FASEB journal : official publication of the Federation of American Societies for Experimental Biology*
9. Broome, C. S., Kayani, A. C., Palomero, J., Dillmann, W. H., Mestril, R., Jackson, M. J., and McArdle, A. (2006) Effect of lifelong overexpression of HSP70 in skeletal muscle on age-related oxidative stress and adaptation after nondamaging contractile activity. *FASEB journal : official publication of the Federation of American Societies for Experimental Biology* **20**, 1549-1551
10. Vasilaki, A., van der Meulen, J. H., Larkin, L., Harrison, D. C., Pearson, T., Van Remmen, H., Richardson, A., Brooks, S. V., Jackson, M. J., and McArdle, A. (2010) The age-related failure of adaptive responses to contractile activity in skeletal muscle is mimicked in young mice by deletion of Cu,Zn superoxide dismutase. *Aging Cell* **9**, 979-990
11. Sataranatarajan, K., Qaisar, R., Davis, C., Sakellariou, G. K., Vasilaki, A., Zhang, Y., Liu, Y., Bhaskaran, S., McArdle, A., Jackson, M., Brooks, S. V., Richardson, A., and Van Remmen, H. (2015) Neuron specific reduction in CuZnSOD is not sufficient to initiate a full sarcopenia phenotype. *Redox Biol* **5**, 140-148
12. Jang, Y. C., Lustgarten, M. S., Liu, Y., Muller, F. L., Bhattacharya, A., Liang, H., Salmon, A. B., Brooks, S. V., Larkin, L., Hayworth, C. R., Richardson, A., and Van Remmen, H. (2010) Increased superoxide in vivo accelerates age-associated muscle atrophy through mitochondrial dysfunction and neuromuscular junction degeneration. *FASEB journal : official publication of the Federation of American Societies for Experimental Biology* **24**, 1376-1390
13. Muller, F. L., Song, W., Liu, Y., Chaudhuri, A., Pieke-Dahl, S., Strong, R., Huang, T. T., Epstein, C. J., Roberts, L. J., 2nd, Csete, M., Faulkner, J. A., and Van Remmen, H. (2006) Absence of CuZn superoxide dismutase leads to elevated oxidative stress and acceleration of age-dependent skeletal muscle atrophy. *Free radical biology & medicine* **40**, 1993-2004

14. Sakellariou, G. K., Jackson, M. J., and Vasilaki, A. (2014) Redefining the major contributors to superoxide production in contracting skeletal muscle. The role of NAD(P)H oxidases. *Free Radic Res* **48**, 12-29
15. Short, K. R., Bigelow, M. L., Kahl, J., Singh, R., Coenen-Schimke, J., Raghavakaimal, S., and Nair, K. S. (2005) Decline in skeletal muscle mitochondrial function with aging in humans. *Proceedings of the National Academy of Sciences of the United States of America* **102**, 5618-5623
16. Vasilaki, A., Mansouri, A., Remmen, H., van der Meulen, J. H., Larkin, L., Richardson, A. G., McArdle, A., Faulkner, J. A., and Jackson, M. J. (2006) Free radical generation by skeletal muscle of adult and old mice: effect of contractile activity. *Aging cell* **5**, 109-117
17. Chabi, B., Ljubicic, V., Menzies, K. J., Huang, J. H., Saleem, A., and Hood, D. A. (2008) Mitochondrial function and apoptotic susceptibility in aging skeletal muscle. *Aging cell* **7**, 2-12
18. Chouchani, E. T., Methner, C., Nadtochiy, S. M., Logan, A., Pell, V. R., Ding, S., James, A. M., Cocheme, H. M., Reinhold, J., Lilley, K. S., Partridge, L., Fearnley, I. M., Robinson, A. J., Hartley, R. C., Smith, R. A., Krieg, T., Brookes, P. S., and Murphy, M. P. (2013) Cardioprotection by S-nitrosation of a cysteine switch on mitochondrial complex I. *Nat Med* **19**, 753-759
19. Anderson, E. J., Lustig, M. E., Boyle, K. E., Woodlief, T. L., Kane, D. A., Lin, C. T., Price, J. W., 3rd, Kang, L., Rabinovitch, P. S., Szeto, H. H., Houmard, J. A., Cortright, R. N., Wasserman, D. H., and Neufer, P. D. (2009) Mitochondrial H2O2 emission and cellular redox state link excess fat intake to insulin resistance in both rodents and humans. *The Journal of clinical investigation* **119**, 573-581
20. Gouspillou, G., Bourdel-Marchasson, I., Rouland, R., Calmettes, G., Biran, M., Deschodt-Arsac, V., Miraux, S., Thiaudiere, E., Pasdois, P., Detaille, D., Franconi, J. M., Babot, M., Trezeguet, V., Arsac, L., and Diolez, P. (2014) Mitochondrial energetics is impaired in vivo in aged skeletal muscle. *Aging cell* **13**, 39-48
21. Lee, H. Y., Choi, C. S., Birkenfeld, A. L., Alves, T. C., Jornayvaz, F. R., Jurczak, M. J., Zhang, D., Woo, D. K., Shadel, G. S., Ladiges, W., Rabinovitch, P. S., Santos, J. H., Petersen, K. F., Samuel, V. T., and Shulman, G. I. (2010) Targeted expression of catalase to mitochondria prevents age-associated reductions in mitochondrial function and insulin resistance. *Cell metabolism* **12**, 668-674
22. Gouspillou, G., Sgarioto, N., Kapchinsky, S., Purves-Smith, F., Norris, B., Pion, C. H., Barbat-Artigas, S., Lemieux, F., Taivassalo, T., Morais, J. A., Aubertin-Leheudre, M., and Hepple, R. T. (2014) Increased sensitivity to mitochondrial permeability transition and myonuclear translocation of endonuclease G in atrophied muscle of physically active older humans. *FASEB journal : official publication of the Federation of American Societies for Experimental Biology* **28**, 1621-1633
23. Pollack, M., and Leeuwenburgh, C. (2001) Apoptosis and aging: role of the mitochondria. *J Gerontol A Biol Sci Med Sci* **56**, B475-482
24. Schriner, S. E., Linford, N. J., Martin, G. M., Treuting, P., Ogburn, C. E., Emond, M., Coskun, P. E., Ladiges, W., Wolf, N., Van Remmen, H., Wallace, D. C., and Rabinovitch, P. S. (2005) Extension of murine life span by overexpression of catalase targeted to mitochondria. *Science* **308**, 1909-1911
25. Perez, V. I., Van Remmen, H., Bokov, A., Epstein, C. J., Vijg, J., and Richardson, A. (2009) The overexpression of major antioxidant enzymes does not extend the lifespan of mice. *Aging cell* **8**, 73-75
26. Wanagat, J., Ahmadieh, N., Bielas, J. H., Ericson, N. G., and Van Remmen, H. (2015) Skeletal muscle mitochondrial DNA deletions are not increased in CuZn-superoxide dismutase deficient mice. *Experimental gerontology* **61**, 15-19
27. McManus, M. J., Murphy, M. P., and Franklin, J. L. (2011) The mitochondria-targeted antioxidant MitoQ prevents loss of spatial memory retention and early neuropathology in a transgenic mouse model of Alzheimer's disease. *J Neurosci* **31**, 15703-15715
28. Rodriguez-Cuenca, S., Cocheme, H. M., Logan, A., Abakumova, I., Prime, T. A., Rose, C., Vidal-Puig, A., Smith, A. C., Rubinsztein, D. C., Fearnley, I. M., Jones, B. A., Pope, S., Heales, S. J., Lam, B. Y., Neogi, S. G., McFarlane, I., James, A. M., Smith, R. A., and Murphy, M. P. (2010) Consequences of long-term oral administration of the mitochondria-targeted antioxidant MitoQ to wild-type mice. *Free Radic Biol Med* **48**, 161-172

29. Lustgarten, M. S., Jang, Y. C., Liu, Y., Muller, F. L., Qi, W., Steinhelper, M., Brooks, S. V., Larkin, L., Shimizu, T., Shirasawa, T., McManus, L. M., Bhattacharya, A., Richardson, A., and Van Remmen, H. (2009) Conditional knockout of Mn-SOD targeted to type IIB skeletal muscle fibers increases oxidative stress and is sufficient to alter aerobic exercise capacity. *American journal of physiology. Cell physiology* **297**, C1520-1532
30. Kuznetsov, A. V., Veksler, V., Gellerich, F. N., Saks, V., Margreiter, R., and Kunz, W. S. (2008) Analysis of mitochondrial function in situ in permeabilized muscle fibers, tissues and cells. *Nature protocols* **3**, 965-976
31. Picard, M., Ritchie, D., Wright, K. J., Romestaing, C., Thomas, M. M., Rowan, S. L., Taivassalo, T., and Hepple, R. T. (2010) Mitochondrial functional impairment with aging is exaggerated in isolated mitochondria compared to permeabilized myofibers. *Aging cell* **9**, 1032-1046
32. Degens, H., Bosutti, A., Gilliver, S. F., Slevin, M., van Heijst, A., and Wust, R. C. (2010) Changes in contractile properties of skinned single rat soleus and diaphragm fibres after chronic hypoxia. *Pflugers Archiv : European journal of physiology* **460**, 863-873
33. Chen, H., Vermulst, M., Wang, Y. E., Chomyn, A., Prolla, T. A., McCaffery, J. M., and Chan, D. C. (2010) Mitochondrial fusion is required for mtDNA stability in skeletal muscle and tolerance of mtDNA mutations. *Cell* **141**, 280-289
34. Changou, C. A., Chen, Y. R., Xing, L., Yen, Y., Chuang, F. Y., Cheng, R. H., Bold, R. J., Ann, D. K., and Kung, H. J. (2014) Arginine starvation-associated atypical cellular death involves mitochondrial dysfunction, nuclear DNA leakage, and chromatin autophagy. *Proceedings of the National Academy of Sciences of the United States of America* **111**, 14147-14152
35. Houot, V., Etienne, P., Petitot, A. S., Barbier, S., Blein, J. P., and Suty, L. (2001) Hydrogen peroxide induces programmed cell death features in cultured tobacco BY-2 cells, in a dose-dependent manner. *Journal of experimental botany* **52**, 1721-1730
36. Sakellariou, G. K., Vasilaki, A., Palomero, J., Kayani, A., Zibrik, L., McArdle, A., and Jackson, M. J. (2013) Studies of Mitochondrial and Nonmitochondrial Sources Implicate Nicotinamide Adenine Dinucleotide Phosphate Oxidase(s) in the Increased Skeletal Muscle Superoxide Generation That Occurs During Contractile Activity. *Antioxid Redox Signal* **18**, 603-621
37. Zielonka, J., and Kalyanaraman, B. (2010) Hydroethidine- and MitoSOX-derived red fluorescence is not a reliable indicator of intracellular superoxide formation: another inconvenient truth. *Free radical biology & medicine* **48**, 983-1001
38. McDonagh, B., Sakellariou, G. K., Smith, N. T., Brownridge, P., and Jackson, M. J. (2014) Differential cysteine labeling and global label-free proteomics reveals an altered metabolic state in skeletal muscle aging. *Journal of proteome research* **13**, 5008-5021
39. Janssen, A. J., Trijbels, F. J., Sengers, R. C., Smeitink, J. A., van den Heuvel, L. P., Wintjes, L. T., Stoltenborg-Hogenkamp, B. J., and Rodenburg, R. J. (2007) Spectrophotometric assay for complex I of the respiratory chain in tissue samples and cultured fibroblasts. *Clinical chemistry* **53**, 729-734
40. Dimauro, I., Pearson, T., Caporossi, D., and Jackson, M. J. (2012) A simple protocol for the subcellular fractionation of skeletal muscle cells and tissue. *BMC Res Notes* **5**, 513
41. Goncalves, R. L., Quinlan, C. L., Perevoshchikova, I. V., Hey-Mogensen, M., and Brand, M. D. (2015) Sites of Superoxide and Hydrogen Peroxide Production by Muscle Mitochondria Assessed ex Vivo under Conditions Mimicking Rest and Exercise. *The Journal of biological chemistry* **290**, 209-227
42. Wang, A. L., Lukas, T. J., Yuan, M., and Neufeld, A. H. (2010) Age-related increase in mitochondrial DNA damage and loss of DNA repair capacity in the neural retina. *Neurobiol Aging* **31**, 2002-2010
43. Mecocci, P., Fano, G., Fulle, S., MacGarvey, U., Shinobu, L., Polidori, M. C., Cherubini, A., Vecchiet, J., Senin, U., and Beal, M. F. (1999) Age-dependent increases in oxidative damage to DNA, lipids, and proteins in human skeletal muscle. *Free radical biology & medicine* **26**, 303-308
44. Miro, O., Casademont, J., Casals, E., Perea, M., Urbano-Marquez, A., Rustin, P., and Cardellach, F. (2000) Aging is associated with increased lipid peroxidation in human hearts, but not with mitochondrial respiratory chain enzyme defects. *Cardiovasc Res* **47**, 624-631

45. Klungland, A., Rosewell, I., Hollenbach, S., Larsen, E., Daly, G., Epe, B., Seeberg, E., Lindahl, T., and Barnes, D. E. (1999) Accumulation of premutagenic DNA lesions in mice defective in removal of oxidative base damage. *Proceedings of the National Academy of Sciences of the United States of America* **96**, 13300-13305
46. Morgan, M. J., and Liu, Z. G. (2011) Crosstalk of reactive oxygen species and NF-kappaB signaling. *Cell research* **21**, 103-115
47. Mukherjee, T. K., Mishra, A. K., Mukhopadhyay, S., and Hoidal, J. R. (2007) High concentration of antioxidants N-acetylcysteine and mitoquinone-Q induces intercellular adhesion molecule 1 and oxidative stress by increasing intracellular glutathione. *J Immunol* **178**, 1835-1844
48. Vasilaki, A., McArdle, F., Iwanejko, L. M., and McArdle, A. (2006) Adaptive responses of mouse skeletal muscle to contractile activity: The effect of age. *Mech Ageing Dev* **127**, 830-839
49. Lee, I. H., Cao, L., Mostoslavsky, R., Lombard, D. B., Liu, J., Bruns, N. E., Tsokos, M., Alt, F. W., and Finkel, T. (2008) A role for the NAD-dependent deacetylase Sirt1 in the regulation of autophagy. *Proc Natl Acad Sci U S A* **105**, 3374-3379
50. Melov, S., Ravenscroft, J., Malik, S., Gill, M. S., Walker, D. W., Clayton, P. E., Wallace, D. C., Malfroy, B., Doctrow, S. R., and Lithgow, G. J. (2000) Extension of life-span with superoxide dismutase/catalase mimetics. *Science* **289**, 1567-1569
51. Sartori, R., Schirwis, E., Blaauw, B., Bortolanza, S., Zhao, J., Enzo, E., Stantzou, A., Mouisel, E., Toniolo, L., Ferry, A., Stricker, S., Goldberg, A. L., Dupont, S., Piccolo, S., Amthor, H., and Sandri, M. (2013) BMP signaling controls muscle mass. *Nature genetics* **45**, 1309-1318
52. McDonagh, B., Sakellariou, G. K., and Jackson, M. J. (2014) Application of redox proteomics to skeletal muscle aging and exercise. *Biochemical Society transactions* **42**, 965-970
53. Doughan, A. K., and Dikalov, S. I. (2007) Mitochondrial redox cycling of mitoquinone leads to superoxide production and cellular apoptosis. *Antioxid Redox Signal* **9**, 1825-1836
54. Asin-Cayuela, J., Manas, A. R., James, A. M., Smith, R. A., and Murphy, M. P. (2004) Fine-tuning the hydrophobicity of a mitochondria-targeted antioxidant. *FEBS Lett* **571**, 9-16
55. Severin, F. F., Severina, II, Antonenko, Y. N., Rokitskaya, T. I., Cherepanov, D. A., Mokhova, E. N., Vyssokikh, M. Y., Pustovidko, A. V., Markova, O. V., Yaguzhinsky, L. S., Korshunova, G. A., Sumbatyan, N. V., Skulachev, M. V., and Skulachev, V. P. (2010) Penetrating cation/fatty acid anion pair as a mitochondria-targeted protonophore. *Proc Natl Acad Sci U S A* **107**, 663-668
56. Patkova, J., Andel, M., and Trnka, J. (2014) Palmitate-induced cell death and mitochondrial respiratory dysfunction in myoblasts are not prevented by mitochondria-targeted antioxidants. *Cell Physiol Biochem* **33**, 1439-1451
57. Fink, B. D., Herlein, J. A., Yorek, M. A., Fenner, A. M., Kerns, R. J., and Sivitz, W. I. (2012) Bioenergetic effects of mitochondrial-targeted coenzyme Q analogs in endothelial cells. *J Pharmacol Exp Ther* **342**, 709-719
58. O'Malley, Y., Fink, B. D., Ross, N. C., Prisinzano, T. E., and Sivitz, W. I. (2006) Reactive oxygen and targeted antioxidant administration in endothelial cell mitochondria. *J Biol Chem* **281**, 39766-39775
59. Dikalov, S., Landmesser, U., and Harrison, D. G. (2002) Geldanamycin leads to superoxide formation by enzymatic and non-enzymatic redox cycling. Implications for studies of Hsp90 and endothelial cell nitric-oxide synthase. *J Biol Chem* **277**, 25480-25485
60. King, M. S., Sharpley, M. S., and Hirst, J. (2009) Reduction of hydrophilic ubiquinones by the flavin in mitochondrial NADH:ubiquinone oxidoreductase (Complex I) and production of reactive oxygen species. *Biochemistry* **48**, 2053-2062
61. Plecita-Hlavata, L., Jezek, J., and Jezek, P. (2009) Pro-oxidant mitochondrial matrix-targeted ubiquinone MitoQ10 acts as anti-oxidant at retarded electron transport or proton pumping within Complex I. *Int J Biochem Cell Biol* **41**, 1697-1707
62. James, A. M., Smith, R. A., and Murphy, M. P. (2004) Antioxidant and prooxidant properties of mitochondrial Coenzyme Q. *Arch Biochem Biophys* **423**, 47-56

Legends to figures

Figure 1. Sarcopenia is associated with myofiber atrophy. A) Age-related changes in anterior tibialis (AT) muscle mass, normalized to body weight (BW). *P<0.05 compared with values from the other age-groups, n=6-8 mice/group. **B**) Transverse section of an AT muscle from an 18 mo old mouse stained with wheat germ agglutinin (WGA, 5μg/ml, red), to visualize extracellular matrix, and assess total fiber numbers and cross-sectional area (CSA) of individual fibers. Scale bar, 500μm. **C**) Number of muscle fibers in AT muscle from 18 and 28 mo old mice. **D**) Average fiber CSA of individual fibers from AT muscle of 18 and 28 mo old mice. *P<0.05 compared with values from 18 mo old mice, n=6-8 mice/group.

Figure 2. Effect of long-term mitoquinone mesylate (MitoQ) administration on mtROS in skeletal muscle of old mice. A) Representative images of a single fiber isolated from the AT muscle under bright field, fluorescent image following loading with MitoSOX Red (20nM, Cyan), and a merged image as indicated and analyzed by confocal microscopy. 60x original magnification. Scale bar, 25μm (top panel); Statistical analysis of the area under the mitochondrial 2-hydroxyethidium (2-OH-Mito-E^+) fluorescence trace (AUC) over 60min for control old mice and mice treated with mitoquinone mesylate (Graphs labelled as MitoQ-treated for brevity throughout) for 15 weeks (from 24 to 28 mo of age), Arbitrary Units (A.U), (bottom panel). 2-OH-Mito-E^+ fluorescence was normalized to CS activity. *P<0.05 compared with values from mitoquinone mesylate-treated old mice, n=12 fibers, 5-6 mice/group. **B**) Confocal images of a saponin-permeabilized fiber isolated from the AT muscle under bright field, fluorescent image following loading with TO-PRO-1 iodide (200nM, Green) and 4',6-diamidino-2-phenylindole (DAPI, 1μg/ml, blue), and a merged image as indicated and analyzed by fluorescence microscopy. 60x original magnification. Scale bar, 25μm. **C**) Mitochondrial hydrogen peroxide (H_2O_2) production (normalized per CS activity) assessed in permeabilized fiber bundles prepared from AT muscle of control and mitoquinone mesylate-treated old mice. Mitochondrial substrates and inhibitors; Glutamate and Malate (G/M, 5mM for both), Succinate (S, 10mM) and Rotenone (Rot, 1μM) were added as indicated in figure. n=5-6 mice/group. **D**) Protein levels of oxidative phosphorylation (OXPHOS) complexes (I, II, III and V) from AT muscle of control and mitoquinone mesylate-treated old mice. The intensity of the bands shown in the Ponceau S-stained gel (top panel) was equivalent to glyceraldehyde 3-phosphate dehydrogenase (GAPDH) and Vinculin protein levels (bottom panel) and were used as loading controls. **E**) Example western blot of GAPDH and voltage-dependent anion channel 3 (VDAC3) content to illustrate the purity of the extracted mitochondrial (Mito) and cytosolic (Cyto) skeletal muscle fractions. **F**) Protein levels of NOX4 in skeletal muscle mitochondrial fractions of control and mitoquinone mesylate-treated old mice. **G**) Rotenone-sensitive respiratory chain complex I activity in AT skeletal muscle homogenates of control and mitoquinone mesylate-treated old mice. n=5-6 mice/group. **H**) Native gels stained for SOD1 and SOD2 enzyme activities in

AT skeletal muscle of control and mitoquinone mesylate-treated old mice (top panel) and densitometric quantification of the bands (bottom panel). Negative control (NC) included AT muscle lysate from Sod1 null mice.

Figure 3. Markers of oxidative damage in skeletal muscle from mitoquinone mesylate (MitoQ) treated old mice. A) Western blot analysis and quantification (bottom right panel) of protein carbonyls in mitochondrial (top right panel) and cytosolic (bottom left panel) skeletal muscle fractions, and AT lysates (top left panel) of control and mitoquinone mesylate-treated old mice. **B**) Western blot analysis (left panel) and quantification (right panel) of 4-hydroxynonenal protein adducts (4-HNE) in mitochondrial (top left panel) and cytosolic skeletal muscle fractions (bottom left panel) of control and mitoquinone mesylate-treated old mice. **C**) Levels of 8-hydroxydeoxyguanosine (8-OHdG) in genomic DNA extracted from skeletal muscle (top left panel), and oxoguanine DNA glycosylase (OGG1) protein levels (bottom panel) of skeletal muscle from control and mitoquinone mesylate-treated old mice and densitometric quantification of the blot (top right panel). n=5-6 mice/group. **D**) 3-nitrotyrosine (3-NT) content (top left panel), and peroxiredoxin V (PRXV) protein levels (bottom panel) of skeletal muscle from control and mitoquinone mesylate-treated old mice and densitometric quantification of the blot (top right panel). n=5-6 mice/group.

Figure 4. Effect of long-term mitoquinone mesylate (MitoQ) treatment on RONS regulatory protein expression in skeletal muscle of old mice. A) Representative western blots depicting superoxide dismutase (SOD) isoform expression in AT lysates and mitochondrial/cytosolic skeletal muscle fractions of control and mitoquinone mesylate-treated old mice. **B**) Protein expression levels of nitric oxide synthase (NOS) isoforms in AT lysates of control and mitoquinone mesylate-treated old mice. **C**) Western blots of the main H_2O_2 reducing enzymes including; catalase (CAT), glutathione peroxidase 1 (GPX1), and peroxiredoxin III (PRXIII) in AT lysates of control and mitoquinone mesylate-treated old mice. **D**) Protein expression of the main redox proteins involved in the thioredoxin-peroxiredoxin system including; thioredoxin 1 and 2 (TRX1 and TRX2), thioredoxin reductase 1 and 2 (TRXR1 and TRXR2) in AT lysates of control and mitoquinone mesylate-treated old mice. **E**) Western blots of heat shock proteins (HSPs) in AT lysates of control and mitoquinone mesylate-treated old mice. **F**) Densitometric analysis of the represented western blots shown in figures (A-E). *$P<0.05$ compared with values from old control mice. **G**) Effect of long-term mitoquinone mesylate treatment on total and phosphorylated IκB-α (Phospho IκB-α) and P65 content (total and phosphorylated), (bottom left panel), and densitometric quantification of the blots (right panel). Coomassie brilliant blue-stained gel (top left panel) served as a loading control, molecular weight marker (M).

Figure 5. Effect of long-term mitoquinone mesylate (MitoQ) administration on mitochondrial content and mitophagy in skeletal muscle of old mice. A) Quantitative RT-PCR measurement of mitochondrial DNA (mtDNA), normalized to the amount of nuclear DNA (nDNA) in skeletal muscle of control and mitoquinone mesylate-treated old mice. n=5-6 mice/group. **B**) Citrate synthase (CS) activity in skeletal muscle of control and mitoquinone mesylate-treated old mice. n=5-6 mice/group. **C**) Representative image of agarose gel electrophoresis of the RT-PCR amplification products of GAPDH, B2M, RPS29, COXI, COXIV, CS, MCIP1, TFAM, PGC1α, NRF1, OPA1, MNF1, MNF2, FIS1, and DRP1 transcripts (top panel). Lanes 1 and 17, 100bp DNA molecular weight marker. The PCR products correspond to the amplicon sizes shown in Table 1. Relative mRNA levels of genes involved in mitochondrial biogenesis and dynamics, analyzed by quantitative RT-PCR (bottom panel). mRNA levels were normalized against the housekeeping genes; GAPDH, B2M and RPS29. **D**) Protein expression of sirtuin 1 (Sirt1) and peroxisome proliferator-activated receptor gamma coactivator-1-alpha (PGC-1α) mitochondrial biogenesis regulators (left panel) in AT skeletal muscle of control and mitoquinone mesylate-treated old mice and densitometric quantification of the blots (right panel). **E**) Western blots of isolated mitochondrial fractions from skeletal muscle of control and mitoquinone mesylate-treated old mice immunodetected for PTEN-induced putative kinase 1 (PINK1), and ubiquitin ligase Parkin, mitophagy markers (left panel), and densitometric quantification of the blots (right panel).

Figure 6. Mitochondrial function in skeletal muscle of mitoquinone mesylate (MitoQ) treated old mice. A) Mitochondrial aconitase (ACONS) activity in AT skeletal muscle of 28 mo old control and mitoquinone mesylate-treated mice. n=5-6 mice/group. **B**) Western blot analysis and quantification (bottom right panel) of ACONS in mitochondrial (top right panel) and cytosolic (bottom left panel) skeletal muscle fractions, and AT lysates (top left panel) of control and mitoquinone mesylate-treated old mice. **C**) Confocal images of a single fiber isolated from the AT muscle under bright field, fluorescent image following loading with Tetramethylrhodamine, methyl ester (TMRM, 20nM, Red) and a merged image as indicated and analyzed by fluorescence microscopy. 60x original magnification. Scale bar, 30μm (top panel); Measurement of $\Delta\Psi m$ in intact mitochondria of isolated AT fibers from control and mitoquinone mesylate-treated old mice, assessed by changes in TMRM fluorescence in response to oligomycin (Olm, 2.5μM) and the protonophore carbonylcyanide-p-trifluoromethoxyphenyl hydrazone (FCCP, 4μM), added at the indicated time points (middle panel); Statistical analysis of the area under the TMRM fluorescence trace (AUC) for control and mitoquinone mesylate-treated old mice (bottom panel). n=10-12 fibers, 5-6 mice/group. **D**) Respiratory function of intact mitochondria in saponin-permeabilized myofibers from control and mitoquinone mesylate-treated old mice shown by changes in respiratory control index (RCI) (left panel), and the ratio of ATP amount to consumed O_2 during state 3 (P:O) ratio (right panel). n=5-6 mice/group. **E**) Uncoupling protein 2 and 3 (UCP2 and 3) protein

levels in skeletal muscle of control and mitoquinone mesylate-treated old mice (left panel) and densitometric quantification of the blots (right panel).

Figure 7. Effect of long-term mitoquinone mesylate (MitoQ) treatment on mitochondrial-mediated apoptosis in skeletal muscle. A) Immunoblots of BAK, BAX and VDAC1 pro-apoptotic proteins in skeletal muscle of control and mitoquinone mesylate-treated old mice (left panel), and densitometric quantification of the blots (right panel). **B**) Protein expression levels of calpain I and calpastatin proteolytic enzymes in muscle of control and mitoquinone mesylate-treated old mice (left panel) and densitometric quantification of the blots (right panel). **C**) Western blots of isolated cytosolic fractions of control and mitoquinone mesylate-treated mice immunodetected for cytochrome c (Cyt C) and Smac/DIABLO mitochondrial pro-apoptotic proteins (left panel), and densitometric quantification of the blots (right panel). **D**) Protein levels of proapoptotic factor endonuclease G (Endo G) in skeletal muscle mitochondrial fractions of control and mitoquinone mesylate-treated old mice (left panel) and densitometric quantification of the blot (right panel). **E**) DNA fragmentation of genomic DNA isolated from skeletal muscle of control and mitoquinone mesylate-treated old mice, analyzed by agarose-gel electrophoresis. Lanes 1 and 10, 1kb DNA molecular weight marker.

Figure 8. Effect of long-term mitoquinone mesylate (MitoQ) treatment on age-related loss of muscle mass and function. A) Time course of the changes in mouse body weight (BW) during the 15-week of mito-targeted mitoquinone mesylate administration. Trend lines indicate no changes in BW during the treatment period, BW was monitored weekly. n=5-6 mice/group. **B**) Transverse sections of AT muscle from 28 mo old control and mitoquinone mesylate-treated mice obtained following the 15-week treatment period, and stained with WGA (5μg/ml, green), to visualize extracellular matrix, and DAPI (1μg/ml, blue), to mark nuclei. Scale bar, 400μm. **C**) Percentage of fibers showing centrally located nuclei in AT muscle of control and mitoquinone mesylate-treated old mice (top left panel); total number of muscle fibers in AT muscle of control and mitoquinone mesylate-treated old mice (top right panel); mean CSA of individual fibers from AT muscle of control and mitoquinone mesylate-treated old mice (bottom panel). n=5-6 mice/group. **D**) Frequency distribution of fiber CSA of AT muscle from control and mitoquinone mesylate-treated old mice. n=5-6 mice/group. **E**) Representative western blots of the fast (MHC fast) and slow (MHC slow) MHC content in gastrocnemius (GTN, top panel) and AT muscle (bottom panel) of control and mitoquinone mesylate-treated old mice. **F**) Maximum isometric specific force measured *in situ,* normalized to total fiber CSA of extensor digitorum longus (EDL) muscle from control and mitoquinone mesylate-treated old mice. n=5-6 mice/group. **G**) *In situ* measurements of the drop in maximum isometric specific force of EDL muscle during a series of repeated isometric contractions (300ms, at 100Hz, every 5s), expressed as a percentage of the initial force. Lines

represent the average response of 5 muscles. n=5 mice/group. Although mitoquinone mesylate-treated old mice showed a tendency to a greater decline in isometric force production during the fatiguing protocol compared with controls, the data were are not statistically significantly. **H**) Image of a skinned myofiber isolated from an AT muscle of a 28 mo old mouse, attached to a force transducer and high-speed length controller. Scale bar, 350μm. **I**) *Ex vivo* measurements of maximum fiber specific force normalized to fiber CSA of skinned myofibers isolated from the AT muscle of control and mitoquinone mesylate-treated old mice. n=25 fibers, 5 mice/group. **J**) *Ex vivo* measurements of the time to peak maximum tension of skinned fibers isolated from the AT muscle of control and mitoquinone mesylate-treated old mice. n=25 fibers, 5 mice/group.

Tables

Table 1. Sequences of the specific primers used for quantitative RT-PCR amplification.

Primer Name (ID)	Forward Primer Sequence	Reverse Primer Sequence	Amplicon Size (bp)
GAPDH	CCGTAGACAAAATGGTGAAGG	TCGTTGATGGCAACAATCTC	109
B2M	GGAGAATGGGAAGCCGAACA	TCTCGATCCCAGTAGACGGT	249
RPS29	ATGGGTCACCAGCAGCTCTA	GTATTTGCGGATCAGACCGT	102
COX I	CACTAATAATCGGAGCCCCA	TTCATCCTGTTCCTGCTCCT	129
COX IV	TGGGAGTGTTGTGAAGAGTGA	GCAGTGAAGCCGATGAAGAAC	273
CS	CAAGATTGTGCCCAATATCCTC	TTCATCTCCGTCATGCCATA	111
MCIP1	CAGCGAAAGTGAGACCAGGG	ACGGGGGTGGCATCTTCTAC	309
TFAM	GCTGATGGGTATGGAGAAG	GAGCCGAATCATCCTTTGC	161
PGC1α	TTCCACCAAGAGCAAGTAT	CGCTGTCCCATGAGGTATT	131
NRF1	TTACTCTGCTGTGGCTGATGG	CCTCTGATGCTTGCGTCGTCT	92
OPA1	TCAGCAAAGCTTACATGCAGA	TGCTTGGACTGGCTACATTTT	180
MFN1	TGCCCTCTTGAGAGATGACC	AGAGCCGCTCATTCACCTTA	182
MFN2	GGGGCCTACATCCAAGAGAG	CCTTGGACAGGTACCCTTTG	115
FIS1	GCCTGGTTCGAAGCAAATAC	CACGGCCAGGTAGAAGACAT	116
DRP1	CTGACGCTTGTGGATTTACC	CCCTTCCCATCAATACATCC	277
ND1	CCTATCACCCTTGCCATCAT	GAGGCTGTTGCTTGTGTGAC	194
PECAM 1	ATGGAAAGCCTGCCATCATG	TCCTTGTTGTTCAGCATCAC	235

GAPDH, glyceraldehyde 3-phosphate dehydrogenase; B2M, beta-2 microglobulin; RPS29, ribosomal protein S29; COX I, cytochrome c oxidase subunit I; COX IV, cytochrome c oxidase subunit IV; CS, citrate synthase; MCIP1, modulatory calcineurin interacting protein-1; TFAM, mitochondrial transcription factor A; PGC1α, peroxisome proliferator-activated receptor α; NRF1, nuclear respiratory factor-1; OPA1, optic atrophy type-1; MFN1, mitofusin-1; MFN2, mitofusin-2; FIS1, mitochondrial fission-1 protein; DRP1, dynamin related protein-1; ND1, mitochondrial encoded NADH dehydrogenase-1; PECAM 1, platelet endothelial cell adhesion molecule-1.

Table 2. Comparison of tissue weights from control and mitoquinone mesylate-treated old mice.

Tissue	Mitoquinone mesylate	Control
BW (gr)	35.2 ± 1.4	33.6 ± 2.6
AT (mg)	43.4 ± 3.4	40.4 ± 2.9
EDL (mg)	10.1 ± 0.5	9.8 ± 0.3
GTN (mg)	154.6 ± 9.9	139.3 ± 6.6
SOL (mg)	9.8 ± 0.7	8.7 ± 0.4
Liver (gr)	1.91 ± 0.16	1.8 ± 0.13
Spleen (mg)	134 ± 21.1	273.3 ± 72.3
Kidney (mg)	273.2 ± 25.9	226.1 ± 12.8
Heart (mg)	211.4 ± 14	195.3 ± 14.5
Lung (mg)	185.2 ± 2.5	175.3 ± 8.9
Brain (mg)	488.8 ± 4.9	468.6 ± 8.9

Values are presented as the mean ± SEM; n= 5-6 mice/group.

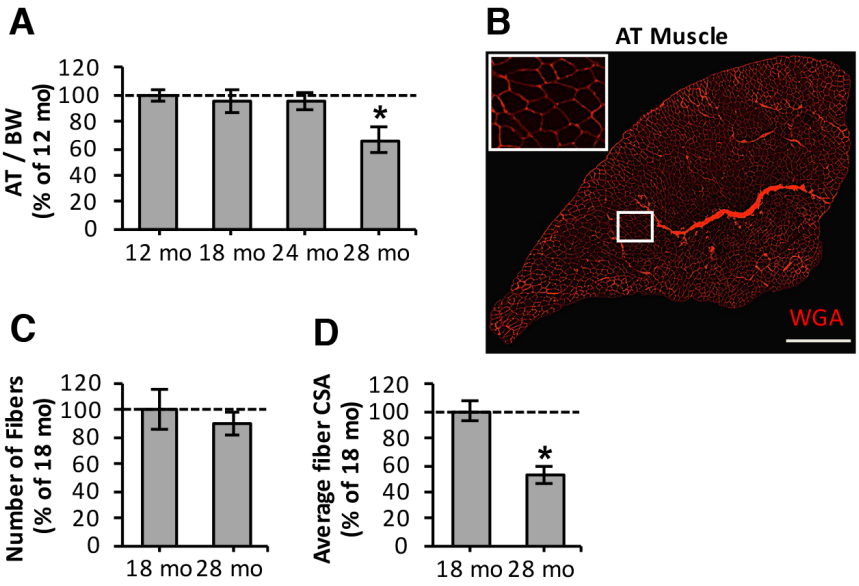
A
AT / BW
(% of 12 mo)
120
100
80
60
40
20
0
*
12 mo 18 mo 24 mo 28 mo
B
AT Muscle
WGA
C
Number of Fibers
(% of 18 mo)
120
100
80
60
40
20
0
18 mo 28 mo
D
Average fiber CSA
(% of 18 mo)
120
100
80
60
40
20
0
*
18 mo 28 mo

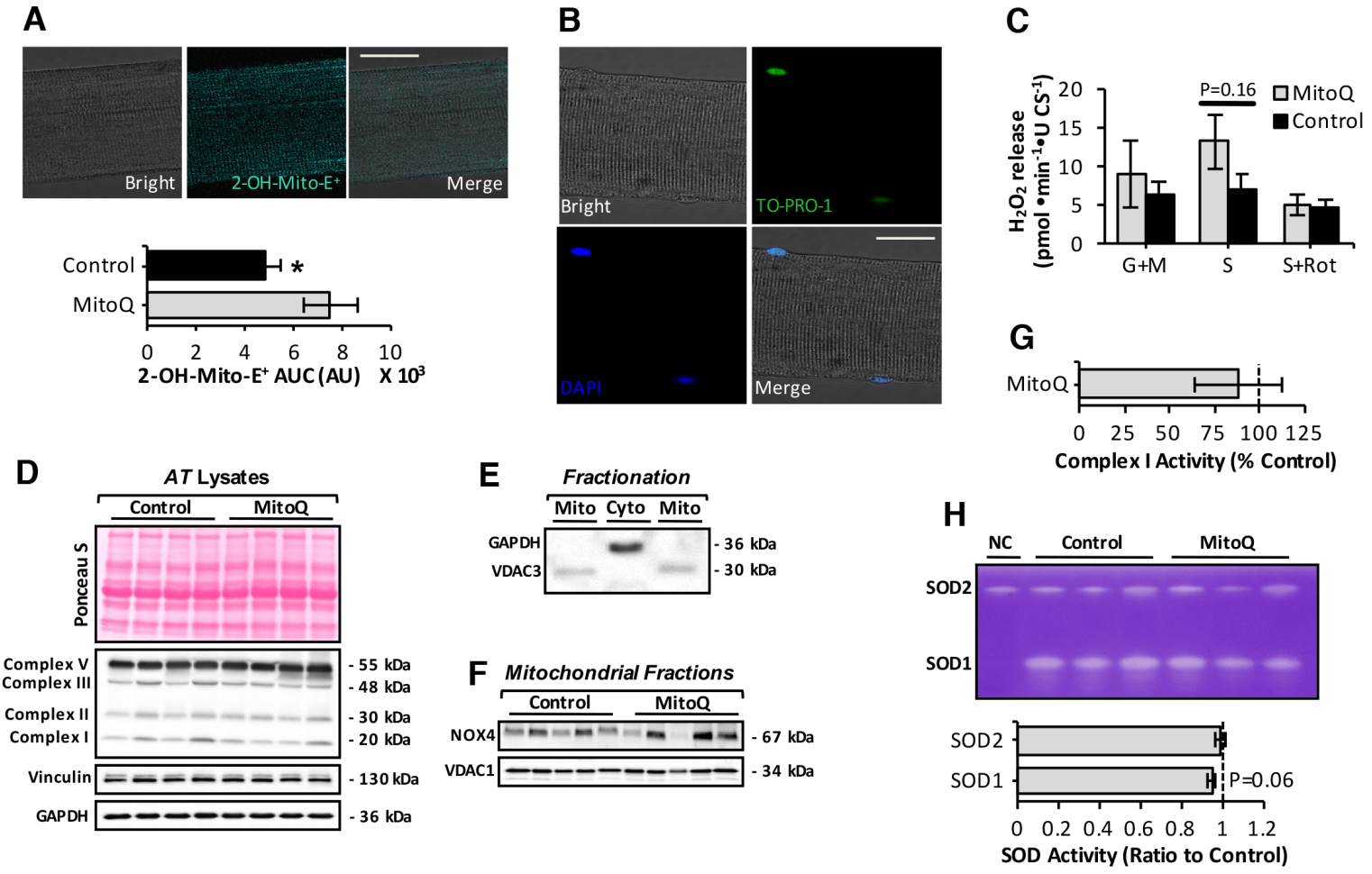
A
Bright
2-OH-Mito-E+
Merge
Control
MitoQ
*
0 2 4 6 8 10
2-OH-Mito-E+ AUC (AU) X 10³
B
Bright
TO-PRO-1
DAPI
Merge
C
H2O2 release (pmol •min-1•U CS-1)
20 15 10 5 0
P=0.16
MitoQ
Control
G+M
S
S+Rot
G
MitoQ
0 25 50 75 100 125
Complex I Activity (% Control)
D
AT Lysates
Control
MitoQ
Ponceau S
Complex V
Complex III
Complex II
Complex I
Vinculin
GAPDH
- 55 kDa
- 48 kDa
- 30 kDa
- 20 kDa
- 130 kDa
- 36 kDa
E
Fractionation
Mito
Cyto
Mito
GAPDH
VDAC3
- 36 kDa
- 30 kDa
F
Mitochondrial Fractions
Control
MitoQ
NOX4
VDAC1
- 67 kDa
- 34 kDa
H
NC
Control
MitoQ
SOD2
SOD1
SOD2
SOD1
P=0.06
0 0.2 0.4 0.6 0.8 1 1.2
SOD Activity (Ratio to Control)

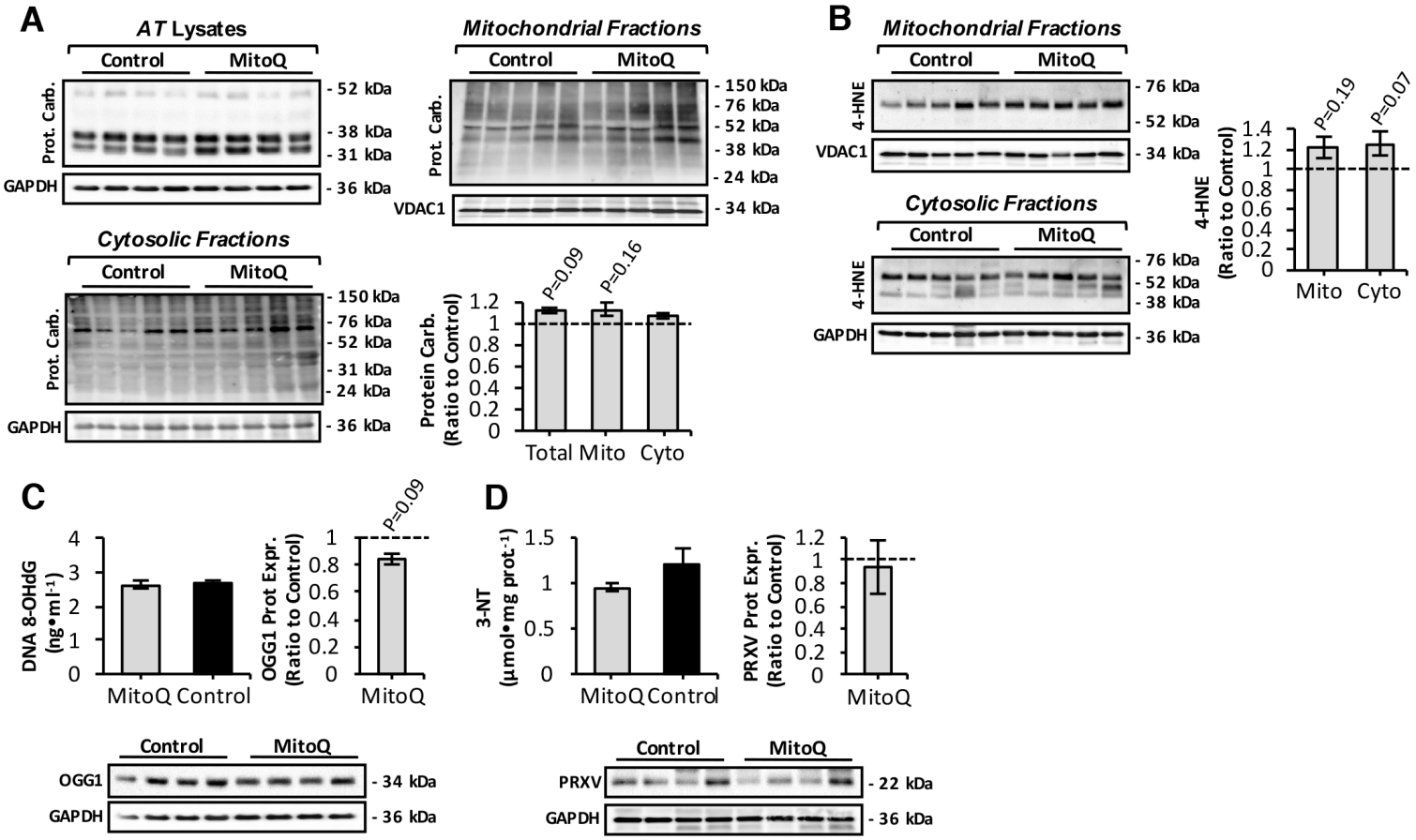
A
AT Lysates
Control
MitoQ
Prot. Carb.
- 52 kDa
- 38 kDa
- 31 kDa
GAPDH
- 36 kDa
Mitochondrial Fractions
Control
MitoQ
Prot. Carb.
- 150 kDa
- 76 kDa
- 52 kDa
- 38 kDa
- 24 kDa
VDAC1
- 34 kDa
Cytosolic Fractions
Control
MitoQ
Prot. Carb.
- 150 kDa
- 76 kDa
- 52 kDa
- 31 kDa
- 24 kDa
GAPDH
- 36 kDa
Protein Carb. (Ratio to Control)
P=0.09
P=0.16
Total Mito Cyto
B
Mitochondrial Fractions
Control
MitoQ
4-HNE
- 76 kDa
- 52 kDa
VDAC1
- 34 kDa
Cytosolic Fractions
Control
MitoQ
4-HNE
- 76 kDa
- 52 kDa
- 38 kDa
GAPDH
- 36 kDa
4-HNE (Ratio to Control)
P=0.19
P=0.07
Mito Cyto
C
DNA 8-OHdG (ng•ml-1)
MitoQ Control
OGG1 Prot Expr. (Ratio to Control)
P=0.09
MitoQ
Control
MitoQ
OGG1
- 34 kDa
GAPDH
- 36 kDa
D
3-NT (µmol•mg prot-1)
MitoQ Control
PRXV Prot Expr. (Ratio to Control)
MitoQ
Control
MitoQ
PRXV
- 22 kDa
GAPDH
- 36 kDa

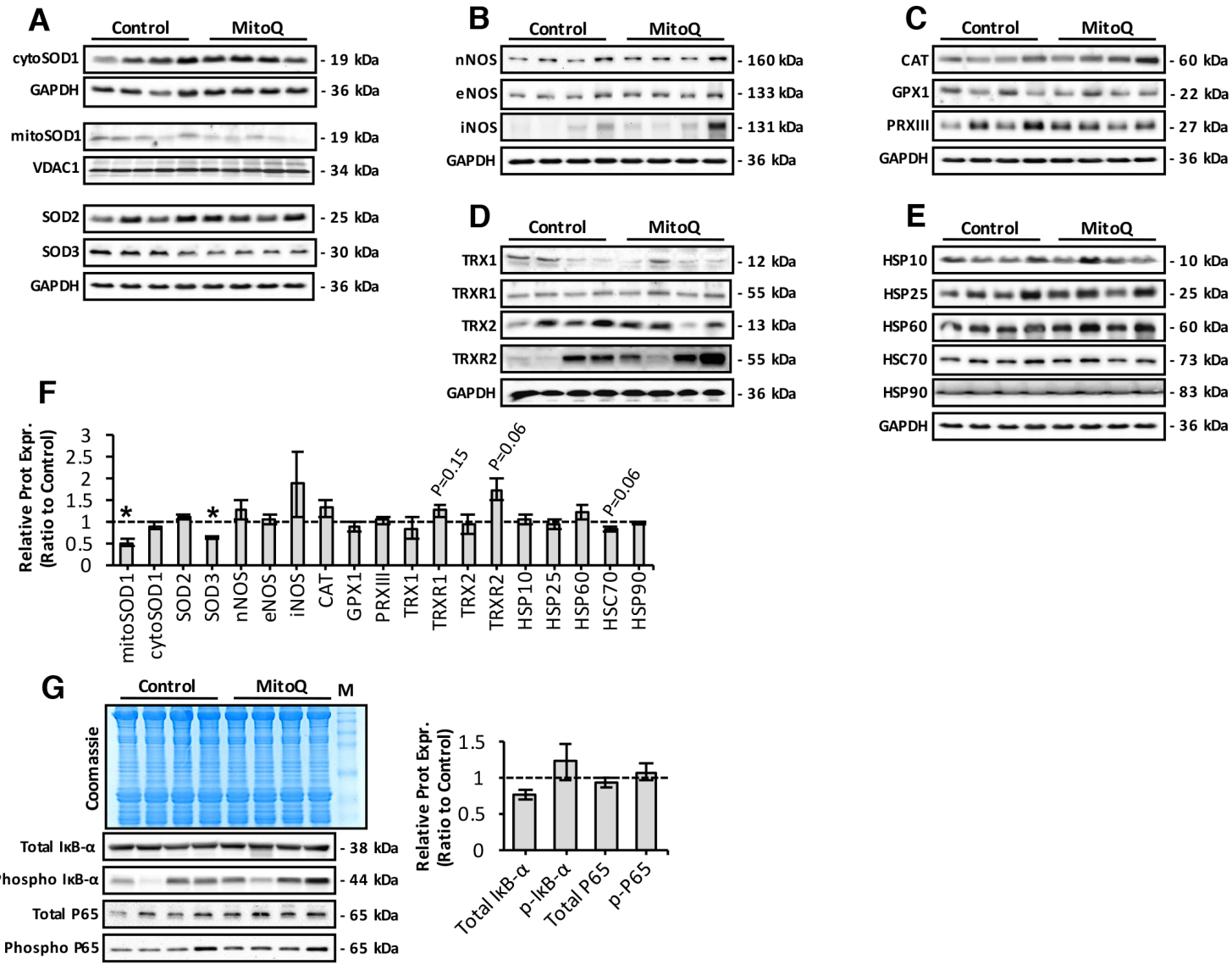
A
Control
MitoQ
cytoSOD1
GAPDH
mitoSOD1
VDAC1
SOD2
SOD3
GAPDH
- 19 kDa
- 36 kDa
- 19 kDa
- 34 kDa
- 25 kDa
- 30 kDa
- 36 kDa
B
Control
MitoQ
nNOS
eNOS
iNOS
GAPDH
- 160 kDa
- 133 kDa
- 131 kDa
- 36 kDa
C
Control
MitoQ
CAT
GPX1
PRXIII
GAPDH
- 60 kDa
- 22 kDa
- 27 kDa
- 36 kDa
D
Control
MitoQ
TRX1
TRXR1
TRX2
TRXR2
GAPDH
- 12 kDa
- 55 kDa
- 13 kDa
- 55 kDa
- 36 kDa
E
Control
MitoQ
HSP10
HSP25
HSP60
HSC70
HSP90
GAPDH
- 10 kDa
- 25 kDa
- 60 kDa
- 73 kDa
- 83 kDa
- 36 kDa
F
Relative Prot Expr. (Ratio to Control)
3
2.5
2
1.5
1
0.5
0
*
*
P=0.15
P=0.06
P=0.06
mitoSOD1
cytoSOD1
SOD2
SOD3
nNOS
eNOS
iNOS
CAT
GPX1
PRXIII
TRX1
TRXR1
TRX2
TRXR2
HSP10
HSP25
HSP60
HSC70
HSP90
G
Control
MitoQ
M
Coomassie
Total IκB-α
Phospho IκB-α
Total P65
Phospho P65
- 38 kDa
- 44 kDa
- 65 kDa
- 65 kDa
Relative Prot Expr. (Ratio to Control)
1.5
1
0.5
0
Total IκB-α
p-IκB-α
Total P65
p-P65

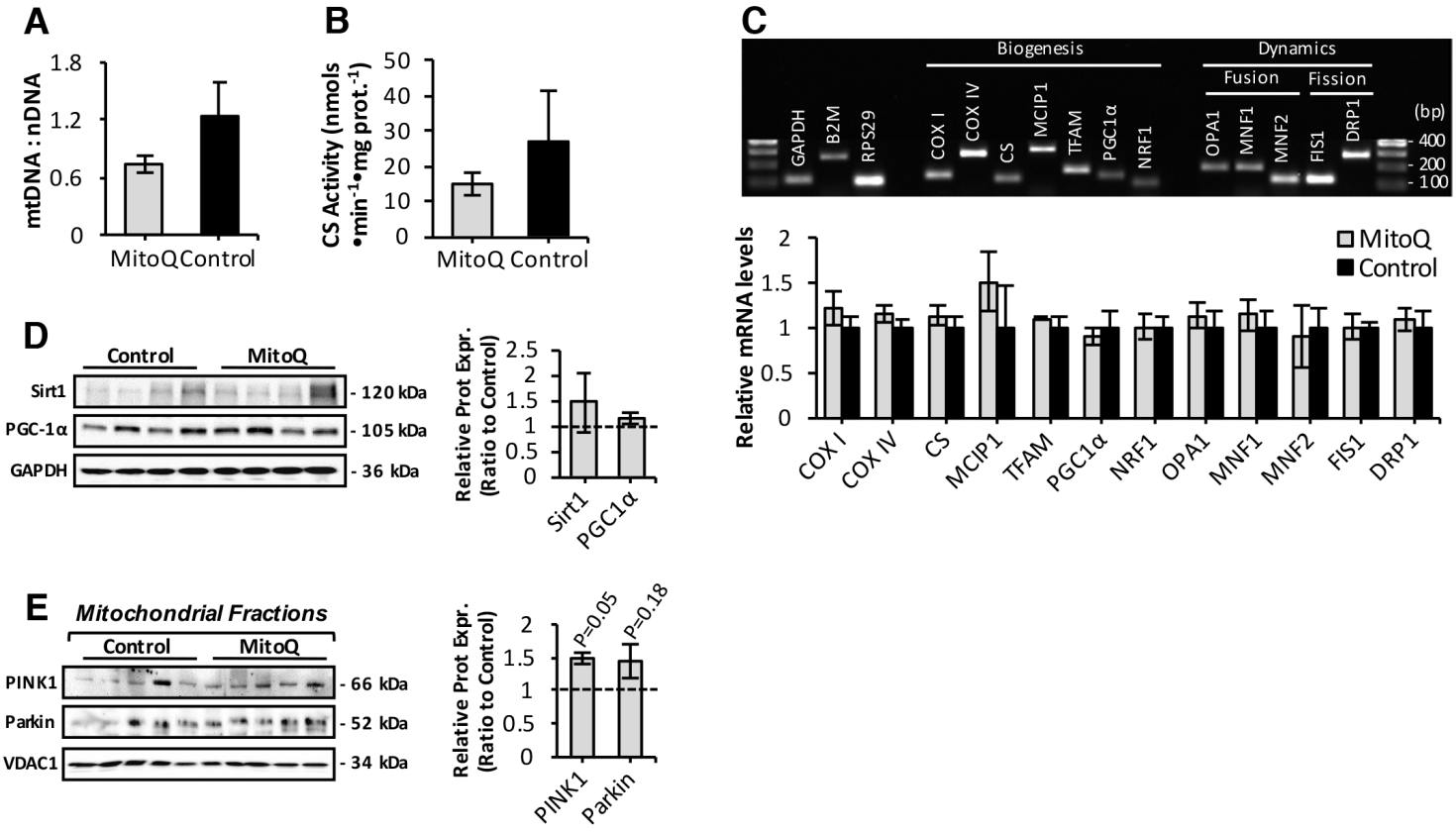
A
mtDNA : nDNA
1.8
1.2
0.6
0
MitoQ Control
B
CS Activity (nmols •min-1•mg prot.-1)
50
40
30
20
10
0
MitoQ Control
C
Biogenesis
Dynamics
Fusion
Fission
GAPDH
B2M
RPS29
COX I
COX IV
CS
MCIP1
TFAM
PGC1α
NRF1
OPA1
MNF1
MNF2
FIS1
DRP1
(bp)
400
200
100
Relative mRNA levels
MitoQ
Control
D
Control
MitoQ
Sirt1
PGC-1α
GAPDH
120 kDa
105 kDa
36 kDa
Relative Prot Expr. (Ratio to Control)
Sirt1
PGC1α
E
Mitochondrial Fractions
Control
MitoQ
PINK1
Parkin
VDAC1
66 kDa
52 kDa
34 kDa
P=0.05
P=0.18
PINK1
Parkin

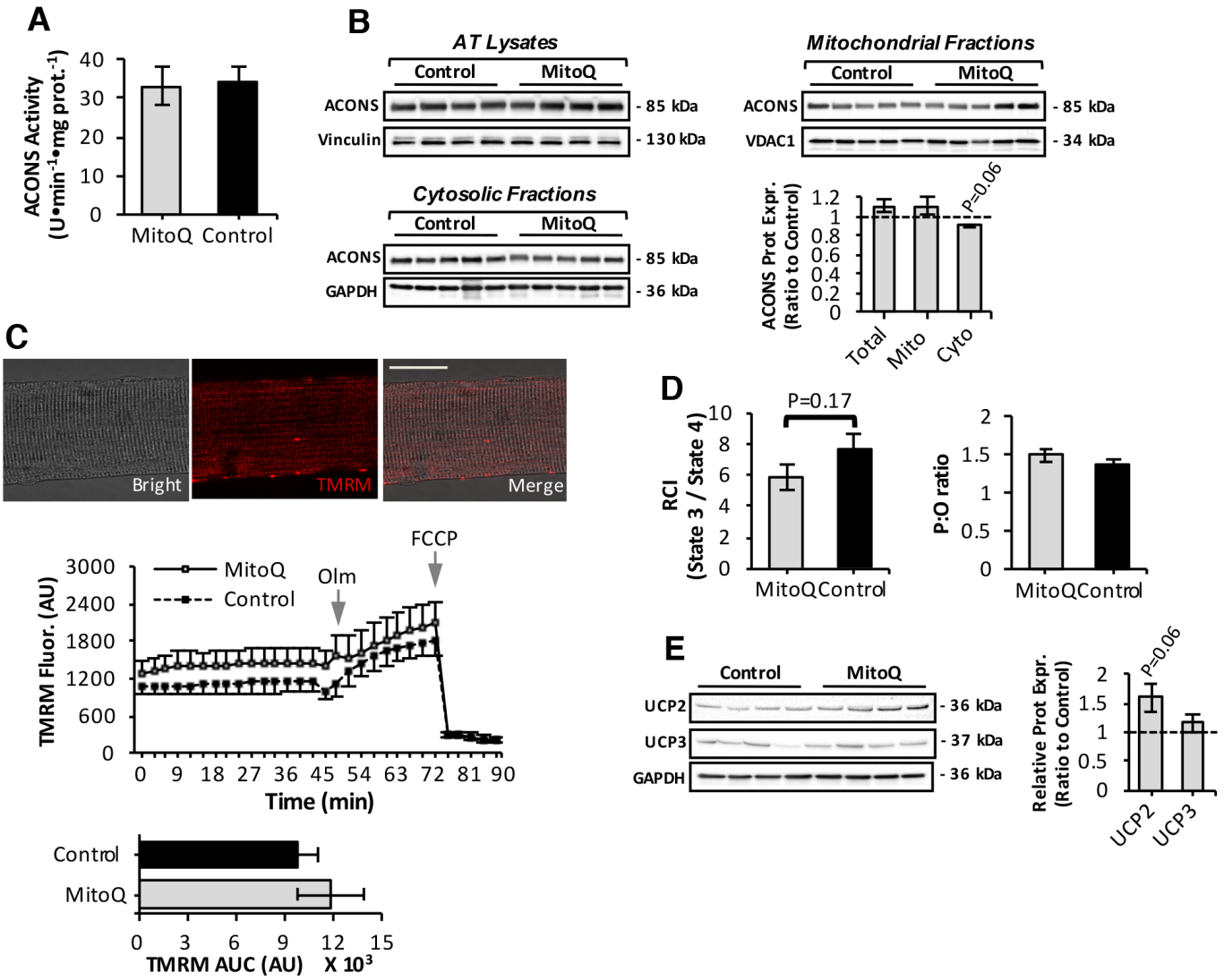
A
ACONS Activity (U•min-1•mg prot.-1)
40
30
20
10
0
MitoQ Control
B
AT Lysates
Control
MitoQ
ACONS
- 85 kDa
Vinculin
- 130 kDa
Cytosolic Fractions
Control
MitoQ
ACONS
- 85 kDa
GAPDH
- 36 kDa
Mitochondrial Fractions
Control
MitoQ
ACONS
- 85 kDa
VDAC1
- 34 kDa
ACONS Prot Expr. (Ratio to Control)
1.2
1
0.8
0.6
0.4
0.2
0
P=0.06
Total
Mito
Cyto
C
Bright
TMRM
Merge
TMRM Fluor. (AU)
3000
2400
1800
1200
600
0
MitoQ
Control
Olm
FCCP
0 9 18 27 36 45 54 63 72 81 90
Time (min)
Control
MitoQ
0 3 6 9 12 15
TMRM AUC (AU) X 10³
D
RCI (State 3 / State 4)
10
8
6
4
2
0
P=0.17
MitoQ Control
P:O ratio
2
1.5
1
0.5
0
MitoQ Control
E
Control
MitoQ
UCP2
- 36 kDa
UCP3
- 37 kDa
GAPDH
- 36 kDa
Relative Prot Expr. (Ratio to Control)
2
1.5
1
0.5
0
P=0.06
UCP2
UCP3

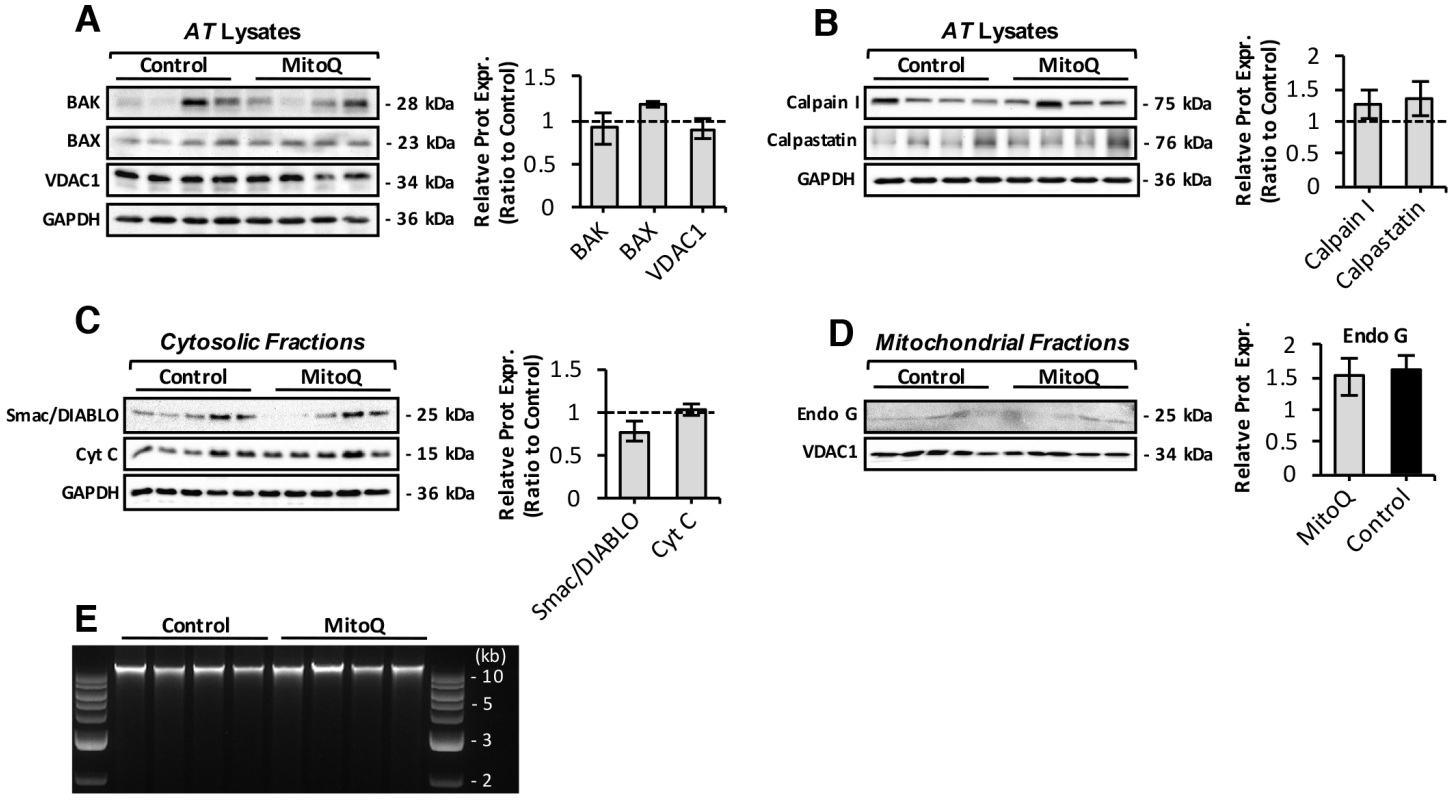
A
AT Lysates
Control
MitoQ
BAK
BAX
VDAC1
GAPDH
- 28 kDa
- 23 kDa
- 34 kDa
- 36 kDa
Relatve Prot Expr. (Ratio to Control)
1.5
1
0.5
0
BAK
BAX
VDAC1
B
AT Lysates
Control
MitoQ
Calpain I
Calpastatin
GAPDH
- 75 kDa
- 76 kDa
- 36 kDa
Relatve Prot Expr. (Ratio to Control)
2
1.5
1
0.5
0
Calpain I
Calpastatin
C
Cytosolic Fractions
Control
MitoQ
Smac/DIABLO
Cyt C
GAPDH
- 25 kDa
- 15 kDa
- 36 kDa
Relative Prot Expr. (Ratio to Control)
1.5
1
0.5
0
Smac/DIABLO
Cyt C
D
Mitochondrial Fractions
Control
MitoQ
Endo G
VDAC1
- 25 kDa
- 34 kDa
Relative Prot Expr.
Endo G
2
1.5
1
0.5
0
MitoQ
Control
E
Control
MitoQ
(kb)
- 10
- 5
- 3
- 2

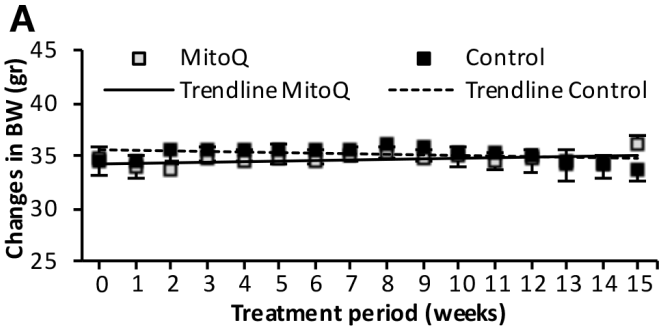
A
MitoQ
Control
Trendline MitoQ
Trendline Control
Changes in BW (gr)
45
40
35
30
25
0 1 2 3 4 5 6 7 8 9 10 11 12 13 14 15
Treatment period (weeks)

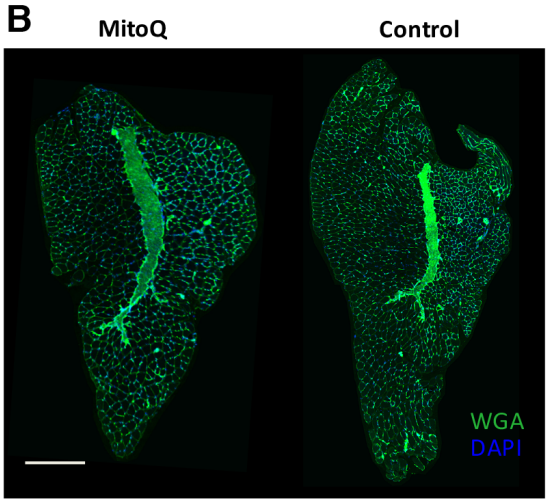
B
MitoQ
Control
WGA
DAPI

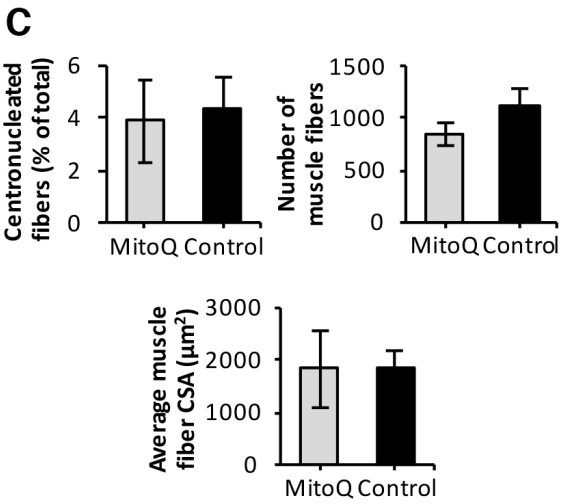
C
Centronucleated fibers (% of total)
6
4
2
0
MitoQ Control
Number of muscle fibers
1500
1000
500
0
MitoQ Control
Average muscle fiber CSA (µm²)
3000
2000
1000
0
MitoQ Control

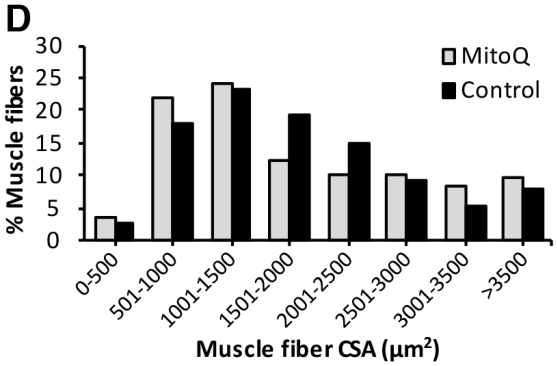
D
% Muscle fibers
30
25
20
15
10
5
0
MitoQ
Control
0-500
501-1000
1001-1500
1501-2000
2001-2500
2501-3000
3001-3500
>3500
Muscle fiber CSA (µm²)

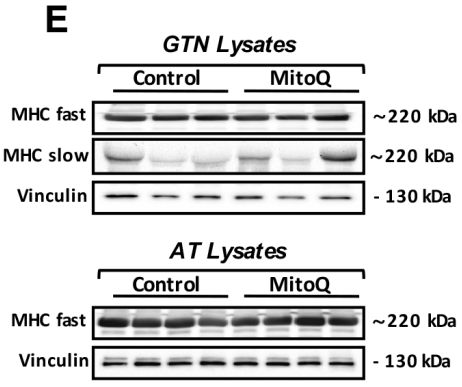
E
GTN Lysates
Control
MitoQ
MHC fast
~220 kDa
MHC slow
~220 kDa
Vinculin
- 130 kDa
AT Lysates
Control
MitoQ
MHC fast
~220 kDa
Vinculin
- 130 kDa

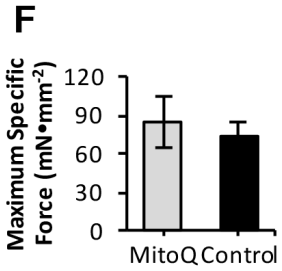
F
Maximum Specific Force (mN•mm⁻²)
120
90
60
30
0
MitoQ Control

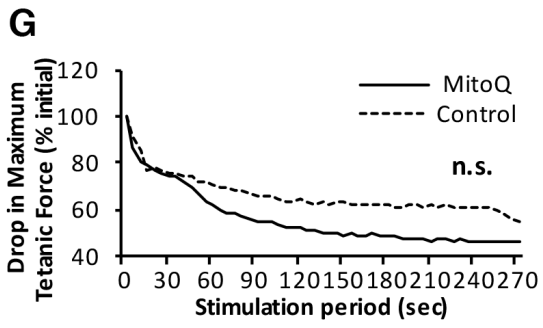
G
Drop in Maximum Tetanic Force (% initial)
120
100
80
60
40
MitoQ
Control
n.s.
0 30 60 90 120 150 180 210 240 270
Stimulation period (sec)

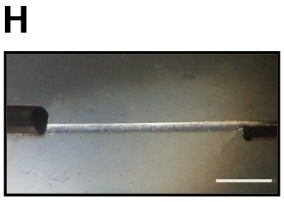
H

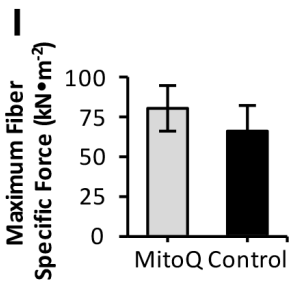
I
Maximum Fiber Specific Force (kN•m⁻²)
100
75
50
25
0
MitoQ Control

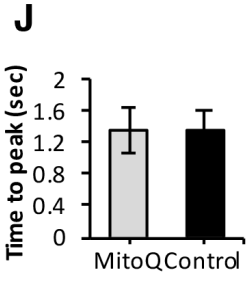
J
Time to peak (sec)
2
1.6
1.2
0.8
0.4
0
MitoQ Control